Accepted Manuscript

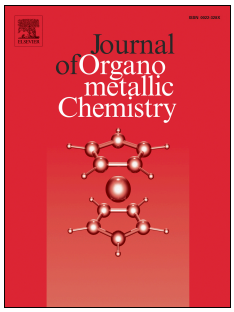

Biological evaluation of new organoruthenium(II) metallates containing 3-acetyl-8-methoxy-2*H*-chromen-2-one appended CNS donor Schiff bases

G. Kalaiarasi, S. Rex Jeya Rajkumar, S. Dharani, Frank R. Fronczek, R. Prabhakaran

PII: S0022-328X(18)30281-X

DOI: 10.1016/j.jorganchem.2018.04.030

Reference: JOM 20422

To appear in: *Journal of Organometallic Chemistry*

Received Date: 5 January 2018

Revised Date: 16 April 2018

Accepted Date: 21 April 2018

Please cite this article as: G. Kalaiarasi, S.R. Jeya Rajkumar, S. Dharani, F.R. Fronczek, R. Prabhakaran, Biological evaluation of new organoruthenium(II) metallates containing 3-acetyl-8-methoxy-2*H*-chromen-2-one appended CNS donor Schiff bases, *Journal of Organometallic Chemistry* (2018), doi: 10.1016/j.jorganchem.2018.04.030.

Biological evaluation of new organoruthenium(II) metallates containing 3-acetyl-8-methoxy-2*H*-chromen-2-one appended CNS donor Schiff bases

G. Kalaiarasi,[a] S. Rex Jeya Rajkumar,[b] S. Dharani,[a] Frank R. Fronczek,[c] and R. Prabhakaran [a*]

[a] *Department of Chemistry, Bharathiar University, Coimbatore 641 046, India.*

[b] *Department of Biosciences and Technology, Karunya University, Coimbatore 641 114, India.*

[c] *Department of Chemistry, Louisiana State University, Baton Rouge, LA 70803, USA*

Abstract

A series of four new, cyclometallated ruthenium(II) complexes was synthesized from 3-acetyl-8-methoxy-2H-chromen-2-one functionalized 4(*N*)- substituted thiosemicarbazones and characterized through various spectral and analytical methods. The molecular structures of the complexes **1**, **2** and **4** were determined by single-crystal X-ray diffraction analysis, which confirmed that the complexes possess a distorted octahedral geometry with the ligands coordinating in a dibasic tridentate fashion via C, N and S atoms. DNA [Calf Thymus DNA (CT-DNA)] and protein [Bovine Serum Albumin (BSA) and Human Serum Albumin (HSA)] binding studies indicated an intercalative mode of binding with DNA and static quenching mechanism with proteins. The compounds cleaved plasmid DNA (pBR322) without application of any external agent and acted well as free radical scavengers. A good spectrum of antimicrobial activity was observed against four bacterial and five fungal pathogens. Two cancerous cell lines, MCF-7 (human breast cancer) and A549 (human lung carcinoma) were employed to test their *in vitro* cytotoxic activity using MTT assay. The complexes (**1-4**) showed better activity with lower IC_{50} values over *cisplatin*. Further non toxic nature of the complexes have been examined with human normal keratinocyte cell line HaCaT. Further, the results of Lactate dehydrogenase release (LDH) and Nitric Oxide (NO) release supported the cytotoxic nature of the compounds. The results of all the biological studies carried out implied that the complex **3** bearing an ethyl substituent was observed to be the best.

Key words: Cyclometallated Ru(II) complexes; DNA/Protein binding; Antimicrobial studies; Cytotoxicity, LDH/NO release.

Corresponding author *Tel.: +91-422-2428319; Fax: +91-422-2422387; E-Mail: rpnchemist@gmail.com* (R. Prabhakaran)

1. Introduction

Development of structurally novel and biologically applicable transition metal complexes is of paramount importance in the field of inorganic research. Increasing attention is on producing metal mediated drugs, primarily with minimal side effects and of highly targeted delivery [1]. Thiosemicarbazide is one such ligand system whose diverse applications *viz*. antitumor, antifungal, antibacterial, antiviral, antiparasitic, etc., have attracted numerous chemists and their activities were found to improve upon complexation with metals [1-6]. They usually have two coordination sites (N and S) and a possibility of an additional donor site greatly enhances their biological and catalytic activities [7]. These Schiff base ligands act as chelating agents and can offer a variety of coordination modes [8]. Coumarin derivatives condensed with thiosemicarbazides provide the above said additional donor site and exhibit noticeable activities. It is a naturally occurring compound widespread in plants. Their anticoagulant and antithrombotic actions were clinically proven. Investigation on coumarin compounds also revealed that they possess antibacterial, antifungal and anticancer properties [9,10]. Coumarin derivatives target a number of pathways in cancer cells such as cell cycle arrest, antimitotic activity, inhibition of kinase, angiogenesis, heat shock protein (HSP90), telomerase, carbonic anhydrase, etc [9]. Novobiocin, clorobiocin and coumermycin A_1 are some of the commercially available coumarin based antibiotics [11,12]. Since coumarins and thiosemicarbazides are individually active in biological processes [2,3,13], the complexation of coumarin thiosemicarbazones with a metal would certainly end up in increased activity. The drawbacks observed with *cisplatin* made the chemists to search for new metal drugs and ruthenium complexes are found to be a better alternative for platinum since it can avail different coordination modes [14], stable oxidation states and mimic iron in binding with biomolecules [15,16]. The synthesis of NAMI-A [17], KP1019 [18], NKP-1339 and their clinical trials in anticancer treatments depicts the effect of ruthenium complexes in chemotherapy [19,20]. Although the potential of ruthenium complexes in therapy is assured, a thorough understanding of their unique modes of action, identification of their biological targets and improving their selectivity are need to be focused still [21]. Demoro *et al* evidenced the anti-trypanosomal [22] and anti-tumour activities [21] of organoruthenium thiosemicarbazone complexes in two separate works. A number of articles are available in displaying the cytotoxic nature of ruthenium(II) complexes, including those reported by Garza-Ortiz *et al* [23], Juinn Chow *et al* [24] and Chang *et al* [25].

The potentiality of reported ruthenium compounds in chemotherapy triggered us to develop new ruthenium based complexes. Our search resulted in the synthesis and evaluation of biological activities of 3-acetyl-8-methoxy coumarin thiosemicarbazones appended Ru(II) complexes.

2. Results and Discussion

2.1. Synthesis and Characterization

The cyclometallated ruthenium(II) complexes were obtained by the direct reaction of the 3-acetyl-8-methoxy-2[H]-chromene-2-one-4(*N*)-substituted thiosemicarbazones (**H_2L^{1-4}**) with [RuHCl(CO)(PPh_3)$_3$] in benzene under reflux conditions, as mentioned in Scheme 1. The complexes were characterized by IR, elemental analyses, UV−Visible, ^{1}H and ^{13}C NMR spectroscopic techniques. The structures of the complexes (**1, 2** and **4**) were confirmed by X-ray crystallography. The ligands were observed to undergo C–H activation at the ortho position of H_3C-C=N, leading to the formation of a five-member metallacycle and behaved as a dibasic tridentate donor. The new complexes (**1–4**) were stable to air and light, non-hygroscopic in nature and were soluble in common organic solvents such as dichloromethane, chloroform, benzene, acetonitrile, ethanol, methanol, dimethylformamide and dimethylsulfoxide and the complexes were stable in aqueous solutions such as 1% aqueous DMSO, phosphate buffer–DMSO (99:1) and Tris-HCl–DMSO (99:1), which was confirmed by UV-Vis spectroscopic techniques (Fig. S1).

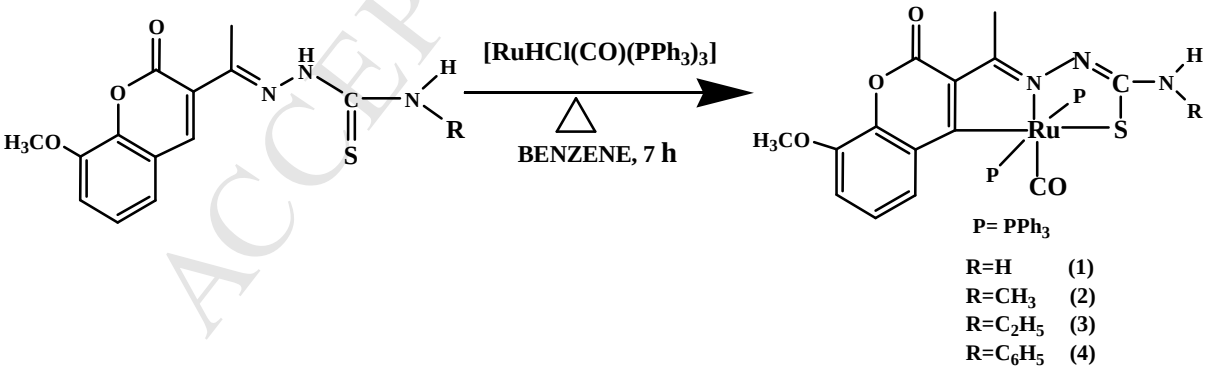

Scheme 1. Synthesis of new Ruthenium(II) Complexes

The IR spectral bands of the new ruthenium(II) complexes (**1-4**) were observed in the ranges 1590-1598 cm^{-1} for C=N stretching vibrations [26] and 729-752 cm^{-1} for C−S stretch [26,27]. The strong band that appeared around 1914-1938 cm^{-1} was assigned to the terminally

coordinated carbonyl group of the complexes **1-4** [26]. In addition, vibrations corresponding to the presence of triphenylphosphine also present in the region 1407-1434, 1089-1090, 694-696 cm^{-1} [20,27].

The electronic spectra of the complexes displayed broad and weak absorption bands in the region around 244−397 nm. The absorption observed at 244-279 nm is most likely due to a transition involving only ligand orbitals ($\pi/\pi^*$and n/π^*) [28]. The bands appearing at around 318–324 nm were assigned to ligand to metal charge transfer transitions [7]. The absorption at 397 nm is probably due to metal to ligand charge transfer transitions [27,28].

The ^{1}H-NMR spectra of the complexes recorded in DMSO showed all the expected signals (Fig.S2–S5). In the spectra of complexes (**1-4**), a singlet appeared in the range of δ 1.88-2.09 ppm has been assigned to the N=C-CH_3 group protons [29]. The ^{1}H-NMR spectra of the complexes confirmed the deprotonation at the C4-H and hydrazinic N(2)H protons of the ligands $\mathbf{H_2L^{1-4}}$ signifying the coordination of ligands in the anionic form after deprotonation at C4 carbon atom of the pyrone ring and enolization and deprotonation of the -NH-C=S group prior to coordination of thiolate sulphur atom [26,27] respectively. All the aromatic protons resonated in the expected range of δ 7.15-7.59 ppm [7] and a singlet corresponding to the –OCH_3 group occurred around δ 3.79-3.91 ppm [30]. A broad singlet appeared at δ 5.74 ppm owing to the NH_2 protons for **1**. In the spectra of the complexes **2**, **3** and **4**, a quatret, triplet and singlet were observed at δ 6.09-6.29, δ 6.63-6.68 and δ 8.49 ppm respectively due to the terminal –NH protons of the substituted thiosemicarbazone ligands H_2L^{2-4} respectively [26]. In the spectra of the complexes (**2** and **3**), a doublet and a triplet was observed around δ 2.10–3.11 and δ 0.73-1.15 ppm due to the methyl group of protons [30]. In addition, a multiplet at δ 2.23–3.60 ppm corresponding to the methylene group of protons was observed in the spectrum of **3** [26].

From the ^{13}C-NMR spectra of the complexes **1-4** (Fig. S6-S9), the carbon resonance signals of C=N group appeared at δ 161.9–166.0 ppm [31]. Peaks at δ 162.9-166.4 ppm were assigned to C-S carbon atom [27,32] and the methoxy carbon appeared at δ 56.1 ppm [30]. Complexes **1-4** exhibited resonance at δ 127.4-133.6 ppm due to the carbon atoms of the triphenylphosphine groups [7]. A singlet at δ 193.6-208.6 ppm is assigned to the terminal carbonyl carbon atom [7,33]. In complexes **2** and **3**, the methyl carbon peak appeared at δ 22.0 and δ 22.1 ppm, respectively, while in complex **3**, the methylene carbon was observed at δ 31.1 ppm [30].

2.2. X-Ray crystallography

The molecular structures of the complexes (**1**, **2** and **4**) have been determined by single crystal X-ray diffraction method and their ORTEP drawings along with the atom numbering scheme are shown in Fig. 1-3. A summary of the structure refinement of the complexes are given in Table 1 and selected bond distances and bond angles of the complexes **1, 2** and **4** are given in Table 2.

2.2.1. Crystal structure description of new Ru(II) complexes

Though attempts were made to obtain crystals of all the four synthesized complexes, crystals suitable for X-ray diffraction studies could be obtained only for complexes **1**, **2** and **4**, and their structures have been solved by X-ray diffraction techniques. From the symmetry of the reflections and the solution of the structures, it is clear that the crystals belong to the orthorhombic system with the P_{212121} space group (complex **1**) and triclinic system with the P-1 space group (complex **2** and **4**). The ORTEP diagrams showed that the thiosemicarbazone ligand is coordinated to the metal ion through the pyrone carbon (C3), N1 hydrazinic nitrogen, and thiolate sulfur atoms with the formation of two five-member ring with a bite angle N(1)−Ru(1)−S(1) of 79.03(9)° for complex **1**, 79.56(5)° for complex **2**, 79.75(3)° for complex **4**, and a bite angle of C(3)-Ru(1)-N(1) of 78.10(14)° for complex **1**, 78.16(8)° for complex **2**, 78.24(4)° for complex **4**. The Ru(1)−N(1) bond distance is 2.091(3) Å for complex **1**, 2.094(2) Å for complex **2**, 2.0844(10) Å for complex **4**, the Ru(1)−S(1) distance is 2.4534(1) Å for complex **1**, 2.4433(7) Å for complex **2**, 2.4334(3) Å for complex **4** and the Ru(1)−C(3) distance is 2.072(4) Å for complex **1**, 2.058(2) Å for complex **2**, 2.061(1) Å for complex **4**. The remaining three sites are occupied by phosphorus atoms of two triphenylphosphine ligands which are mutually *trans* to each other with Ru(1)−P(1) and Ru(1)−P(2) distances of 2.3759(11) Å and 2.3844(12) Å for complex **1**, 2.3780(7) Å and 2.3582(6) Å for complex **2**, 2.3664(3) Å and 2.3717(3) Å for complex **4**, and a carbonyl group with Ru(1)−C(14) distances of 1.851(4) Å for complex **1**, Ru(1)−C(15) distances of 1.846(2) Å for complex **2**, Ru(1)−C(20) distances of 1.8564(12) Å for complex **4**. The *trans* arrangement of bulky triphenylphosphine ligands may be due to the presence of CO, a stronger π-acidic ligand that completes the hexa coordination, might have forced the bulky triphenylphosphine to take *trans* position for steric reasons. The observed bond distances are comparable with those found in other reported ruthenium complexes containing triphenylphosphine [7,16,22,26,34,35]. This bond lengthening could be attributed to the

strong trans influence of the bulkier triphenylphosphine ligands. The two triphenylphosphine ligands which are mutually *trans* to each other and are slightly bent towards the carbonyl group due to the steric requirements of somewhat bulky chelating ligand, causing a slight deviation from a linear *trans* arrangement, which is evident from the bond angle of P(1)–Ru(1)–C(14)= 87.4(1)° for complex **1**, P(1)–Ru(1)–C(15)= 89.46(8)° for complex **2**, P(1)–Ru(1)–C(20)= 89.12(4)° for complex **4**, are smaller than bond angle of P(1)–Ru(1)–N(1)= 89.92(9)° for complex **1**, P(1)–Ru(1)–N(1)= 89.62(6)° for complex **2**, P(1)–Ru(1)–N(1)= 90.07(3)° for complex **4**, and P(2)–Ru(1)–N(1)= 92.01(9)° for complex **1**, P(2)–Ru(1)–N(1)= 90.56(6)° for complex **2**, P(2)–Ru(1)–N(1)= 92.01(3)° for complex **4**. The carbonyl group occupies the site *trans* to N(1). The *cis* bond angles found in the complexes agree well with those reported for similar ruthenium complexes [7,16,26,34,35]. The *trans* angles C(14)−Ru(1)−N(1) = 176.84(15)° for complex **1**, C(15)−Ru(1)−N(1) = 178.39(9)° for complex **2**, C(20)−Ru(1)−N(1) = 177.76(4)° for complex **4**, P(2)−Ru−P(1) = 174.82(4)° for **1**, 176.46(2)° for **2**, 174.65(11)° for **3** and S(1)−Ru(1)−C(3) = 156.83(12)° for **1**, 157.61(7)° for **2** and 157.97(3)° for **4**, deviated from linearity. The distorted octahedron is evidenced by the longer Ru–P bonds when compared to the equatorial bonds and also the deviation from the corresponding *cis* and *trans* bond angles of 90° and 180°.

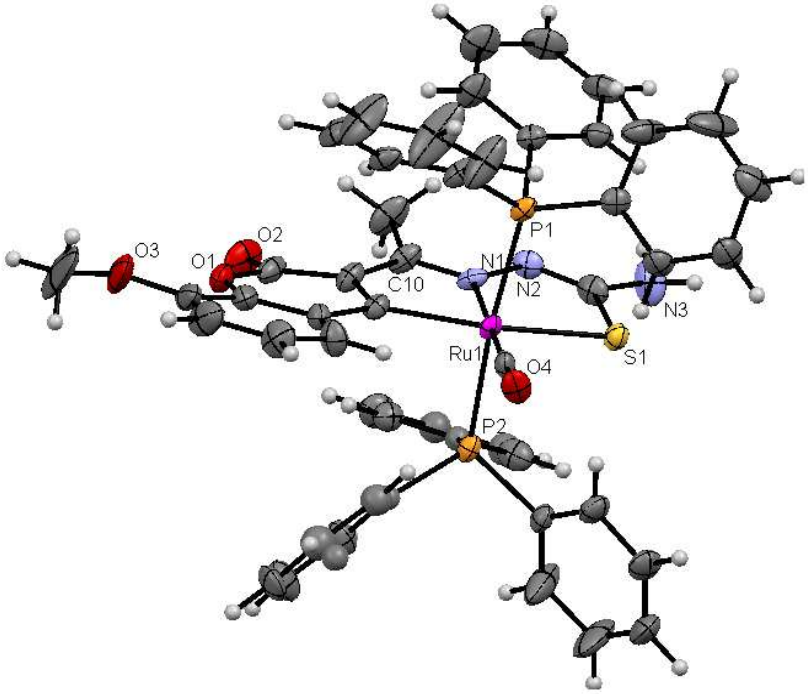

Fig. 1. ORTEP diagram of **[Ru(8MAC-tsc)CO(PPh$_3$)$_2$]** (**1**)

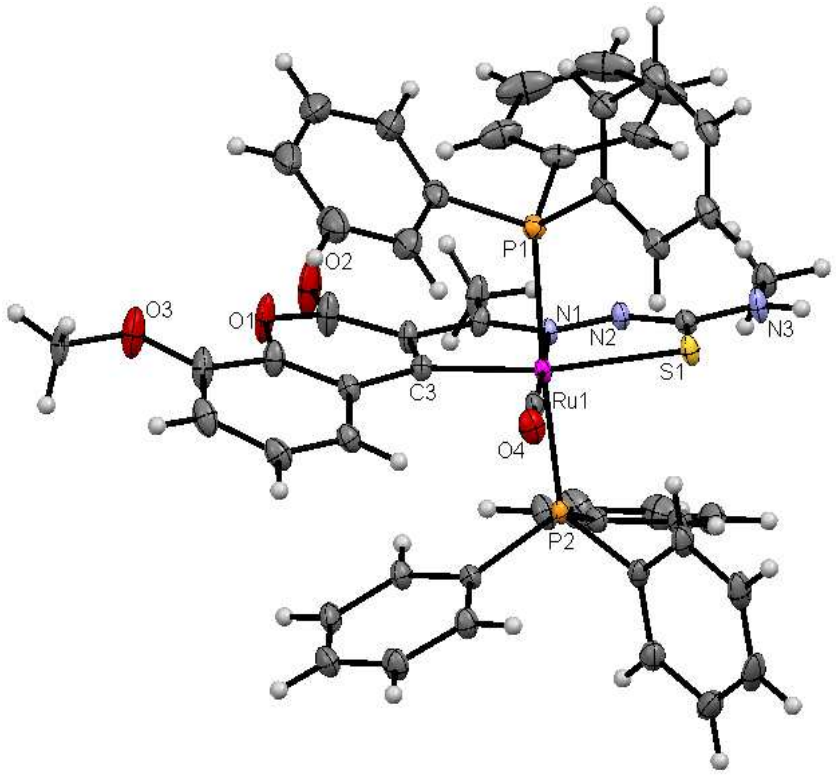

Fig. 2. ORTEP diagram of **[Ru(8MAC-mtsc)CO(PPh$_3$)$_2$]** (**2**)

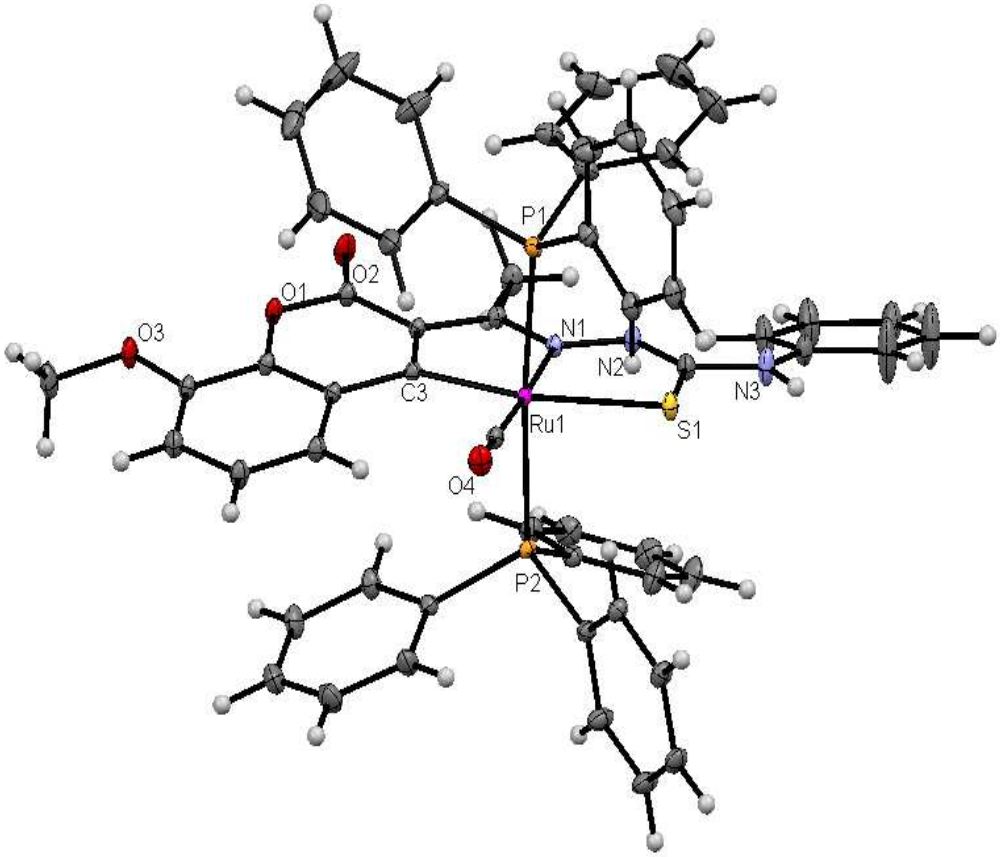

Fig. 3. ORTEP diagram of **[Ru(8MAC-ptsc)CO(PPh$_3$)$_2$]** (**4**)

Table 1. Crystallographic data of the complexes (**1, 2** and **4**)

Identification code	[Ru(8MAC-tsc)CO(PPh_3)$_2$]	[Ru(8MAC-mtsc)CO(PPh_3)$_2$]	[Ru(8MAC-ptsc)CO(PPh_3)$_2$]
Empirical formula	$C_{50}H_{41}N_3O_4P_2RuS$	$C_{51}H_{43}N_3O_4P_2RuS.(0.34)H_2O$	$C_{56}H_{45}N_3O_4P_2RuS.(0.5)CH_2Cl_2$
Formula weight	942.93	962.99	1061.48
Temperature	90.0(5) K	90.0(5) K	90.0(5) K
Wavelength	0.71073 Å	0.71073 Å	0.71073 Å
Crystal system	Orthorhombic	Triclinic	Triclinic
Space group	*P*212121	P -1	P-1
Unit cell dimensions			
a	16.648(3) Å	10.9779(3) Å	13.2638(6) Å
b	10.358(2)Å	11.5073(3) Å	13.3525(6) Å
c	24.080(5) Å	17.6704(5) Å	14.2108(7) Å
α	90°	86.8063 °	86.438(2) °
β	90°	83.3108 °	86.217(2) °
γ	90°	88.4161 °	71.830(2) °
Volume	4152.4(14) $Å^3$	2213.09(10) $Å^3$	2383.80(19) $Å^3$
Z	4	2	2
Density	1.508 Mg/m^3	1.445 Mg/m^3	1.479 Mg/m^3
Absorption coefficient	0.557 mm^{-1}	0.525 mm^{-1}	0.548 mm^{-1}
F(000)	1936	991	1090
Crystal size	0.18 × 0.13 × 0.05 mm	0.21 × 0.20 × 0.05 mm	0.27 × 0.23 × 0.08 mm
Crystal shape	plate	Plate	Lath
θ range for data collection	1.487 to 26.799 °	1.868 to 30.029 °	1.437 to 34.996 °
Limiting indices	-20≤*h*≤ 21, -13 ≤*k*≤ 12, -30 ≤*l*≤ 27	-15 ≤*h*≤ 15, -16 ≤*k*≤ 16, -24 ≤*l*≤ 24	-21 ≤*h*≤ 21, -21≤*k*≤ 20, -22 ≤*l*≤ 22
Independent reflections	63045 (R(int)=0.0699)	12872 (R(int)=0.0300)	71724 (R(int)=0.0220)
Absorption correction	multi-scan	multi-scan	multi-scan
Refinement method	Full-matrix least-squares on F^2	Full-matrix least-squares on F^2	Full-matrix least-squares on F^2
Data/Restraints/ Parameters	63045/2/565	12872/3/588	71724/2/636
Goodness-of-fit on F^2	1.026	1.006	1.029
Final *R* indices [$I>2\sigma(I)$]	R1 = 0.0323, wR2= 0.0700	R1 = 0.0429, wR2= 0.0890	R1 = 0.0315, wR2= 0.0837
R indices (all data)	R1 = 0.0418, wR2 = 0.0663	R1 = 0.0706, wR2 = 0.1008	R1 = 0.0384, wR2 = 0.0881

Table 2. Selected bond lengths (Å) and bond angles (°) of the complexes (**1, 2** and **4**)

BOND LENGTHS					
1		**2**		**4**	
Ru1 C14	1.851(4)	Ru1 C15	1.846(2)	Ru1 C20	1.8564(12)
Ru1 C3	2.072(4)	Ru1 C3	2.058(2)	Ru1 C3	2.0616(11)
Ru1 N1	2.091(3)	Ru1 N1	2.094(2)	Ru1 N1	2.0844(10)
Ru1 P1	2.376(1)	Ru1 P1	2.3780(7)	Ru1 P1	2.3664(3)
Ru1 P2	2.385(1)	Ru1 P2	2.3582(6)	Ru1 P2	2.3717(3)
Ru1 S1	2.453(1)	Ru1 S1	2.4433(7)	Ru1 S1	2.4334(3)
BOND ANGLES					
1		**2**		**4**	
S1 Ru1 C14	102.51(12)	S1 Ru1 C15	102.04(7)	S1 Ru1 C20	101.52(4)
S1 Ru1 C3	156.83(1)	S1 Ru1 C3	157.61(7)	S1 Ru1 C3	157.97(4)
S1 Ru1 N1	79.03(9)	S1 Ru1 N1	79.56(5)	S1 Ru1 N1	79.75(3)
S1 Ru1 P1	89.25(4)	S1 Ru1 P1	88.00(2)	S1 Ru1 P1	88.38(1)
S1 Ru1 P2	86.40(4)	S1 Ru1 P2	88.55(2)	S1 Ru1 P2	86.66(1)
P1 Ru1 C3	94.6(1)	P1 Ru1 C3	89.59(7)	P1 Ru1 C3	92.42(3)
P1 Ru1 N1	89.92(9)	P1 Ru1 N1	89.62(6)	P1 Ru1 N1	90.07(3)
P1 Ru1 P2	174.82(4)	P1 Ru1 P2	176.45(2)	P1 Ru1 P2	174.66(2)
P1 Ru1 C14	87.4(1)	P1 Ru1 C15	89.46(7)	P1 Ru1 C20	88.12(4)
P2 Ru1 C14	90.85(12)	P2 Ru1 C15	90.46(7)	P2 Ru1 C20	90.90(4)
P2 Ru1 C3	90.55(11)	P2 Ru1 C3	93.91(7)	P2 Ru1 C3	92.92(3)
P2 Ru1 N1	92.01(9)	P2 Ru1 N1	90.56(6)	P2 Ru1 N1	91.02(3)
N1 Ru1 C14	176.8(1)	N1 Ru1 C15	178.39(9)	N1 Ru1 C20	177.76(5)
N1 Ru1 C3	78.1(1)	N1 Ru1 C3	78.16(8)	N1 Ru1 C3	78.24(4)
C3 Ru1 C14	100.5(2)	C3 Ru1 C15	100.2(1)	C3 Ru1 C20	100.51(5)
C11 S1 Ru1	94.9(2)	C11 S1 Ru1	95.44(8)	C11 S1 Ru1	95.20(4)
C15 P1 Ru1	117.2(1)	C16 P1 Ru1	117.82(8)	C33 P1 Ru1	112.18(4)
C21 P1 Ru1	115.7(1)	C22 P1 Ru1	115.99(8)	C21 P1 Ru1	116.06(4)
C27 P1 Ru1	113.4(1)	C28 P1 Ru1	111.11(8)	C27 P1 Ru1	117.07(4)
C33 P2 Ru1	116.8(1)	C34 P2 Ru1	113.25(8)	C39 P2 Ru1	114.18(4)
C39 P2 Ru1	106.5(2)	C40 P2 Ru1	117.45(8)	C45 P2 Ru1	112.12(4)
C45 P2 Ru1	118.1(2)	C46 P2 Ru1	111.78(8)	C51 P2 Ru1	116.47(4)
N2 N1 Ru1	125.0(2)	N2 N1 Ru1	124.5(1)	N2 N1 Ru1	124.55(8)
C10 N1 Ru1	118.3(3)	C10 N1 Ru1	118.1(2)	C10 N1 Ru1	118.28(8)
C2 C3 Ru1	112.1(3)	C2 C3 Ru1	113.0(2)	C2 C3 Ru1	112.85(8)
C4 C3 Ru1	132.6(3)	C4 C3 Ru1	130.7(2)	C4 C3 Ru1	130.99(9)
O4 C14 Ru1	177.5(3)	O4 C15 Ru1	178.5(2)	O4 C20 Ru1	176.78(1)

While dealing with the hydrogen-bonding interaction, in complex (**2**), we found the donor–acceptor interactions between the O(2) oxygen atom of the molecule with O(5) oxygen atom of the water came from solvent of crystallisation O(2)----O(5)= 3.015 Å (Fig. 4; Table S1). In complex (**4**) we found the donor–acceptor distance (3.006 Å) corresponding to the

O(4)-O(4) bond between the carbonyl oxygen atom of the first molecule and the carbonyl oxygen atom of the second molecule. This interaction gave a pseudo binuclear structural appearance to the complex **4** (Fig. 5; Table S1).

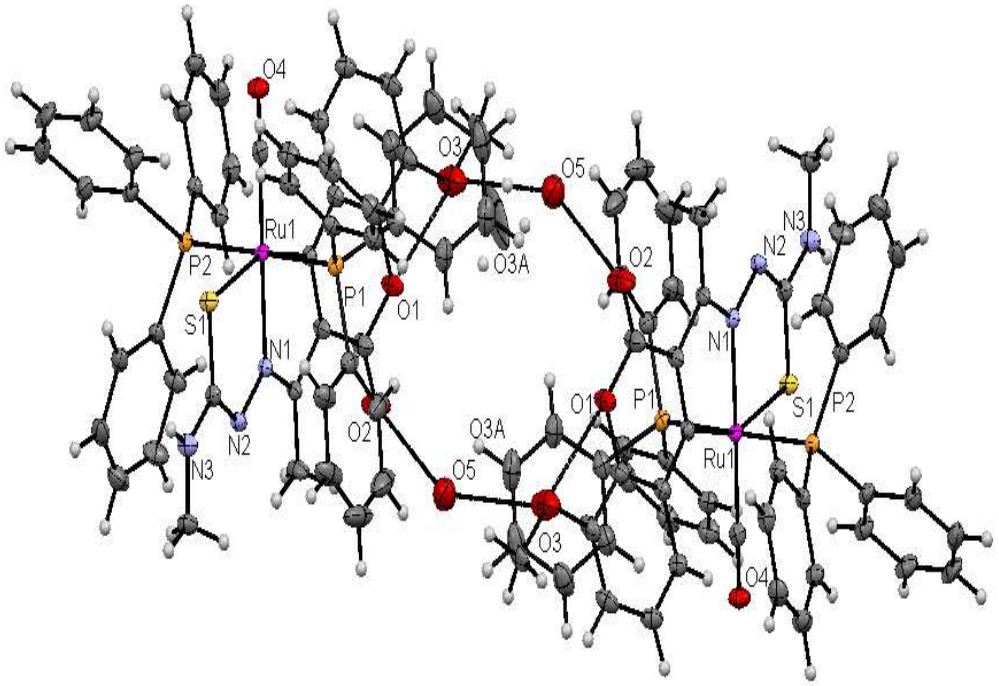

Fig. 4. ORTEP diagram of **[Ru(8MAC-mtsc)CO(PPh$_3$)$_2$] (2)** with hydrogen bonding

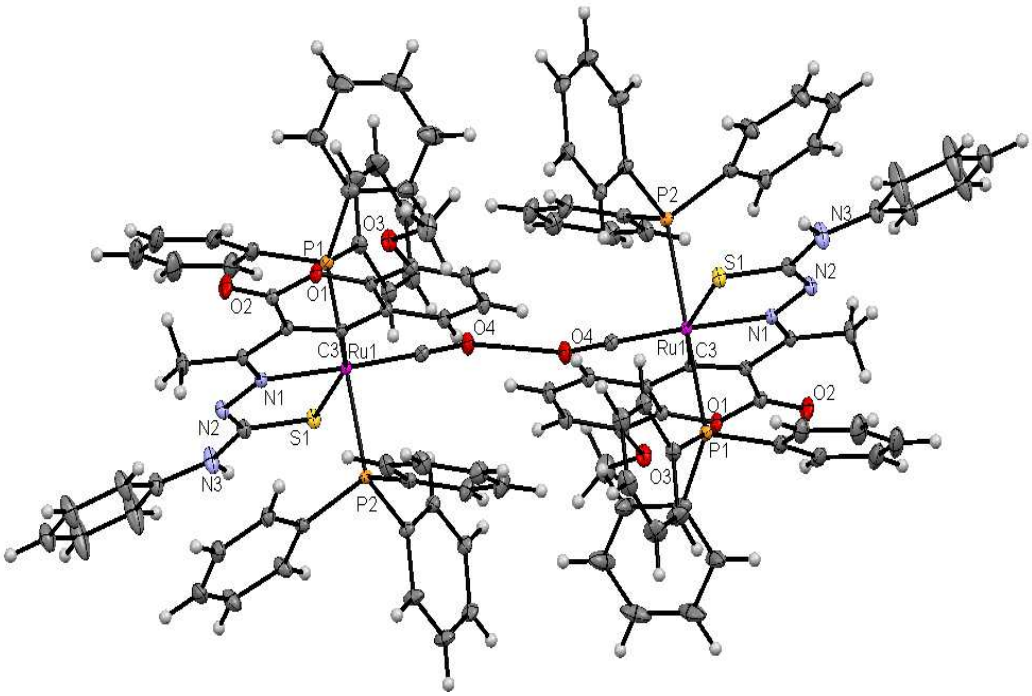

Fig. 5. ORTEP diagram of **[Ru(8MAC-ptsc)CO(PPh$_3$)$_2$] (4)** with hydrogen bonding

2.3. DNA binding studies

2.3.1. UV–Vis absorption spectral titrations

The electronic absorption spectra of the complexes **1–4** (25 µM) in the absence and presence of CT-DNA (2.5–25 µM) are depicted in Fig. 6. By using absorption spectral technique, the intrinsic binding constant (K_b) value of the compounds was determined from the absorptivity changes of the respective compounds upon the incremental addition of CT-DNA. The LMCT absorption band of the complex **1** at 322 nm exhibited a hypochromism of about 31.91 % with a red shift of 3 nm. The absorption bands of complex **2** and **3** showed hypochromism of about 39.06 % and 44.04 % with a bathochromic shift of 3 nm and 4 nm at 322 and 320 nm respectively. Whereas, the absorption bands of the complex **4** at 283 nm and 393 nm exhibited the same phenomenon of hypochromism of about 31.42 % and 34.74 %, with a red shift of about 3 nm. The decrease in absorbance with increase in concentration of CT-DNA may be due to the decrease in transition probabilities as a result of partial transfer of electrons from the π orbital of the DNA base pairs to the coupled π* orbital of the coordinated Schiff base to metal due to overlapping [36]. The extent of hypochromism in the charge transfer band is an indication of the strength of intercalative interaction [36]. Above spectral results obviously inferred that the complexes interact with CT-DNA via intercalation mode. The intrinsic binding constant K_{bin} was calculated from the ratio of slope to the y intercept in plots of [DNA]/[$\varepsilon_a - \varepsilon_f$] versus [DNA] (Inset of Fig. 6) and are given in Table 3. The obtained binding constant values showed that the cyclometallated Ru(II) complexes behaved as potent binders to DNA through intercalation and the order of binding affinity of the complexes with CT-DNA is **3** > **2** > **1** > **4**. This may be due to the presence of different substitutents in the terminal nitrogen atom of the ligands. These results are comparable with earlier reports describing the intercalative mode of various ruthenium intercalators [20,26,34,37-39].

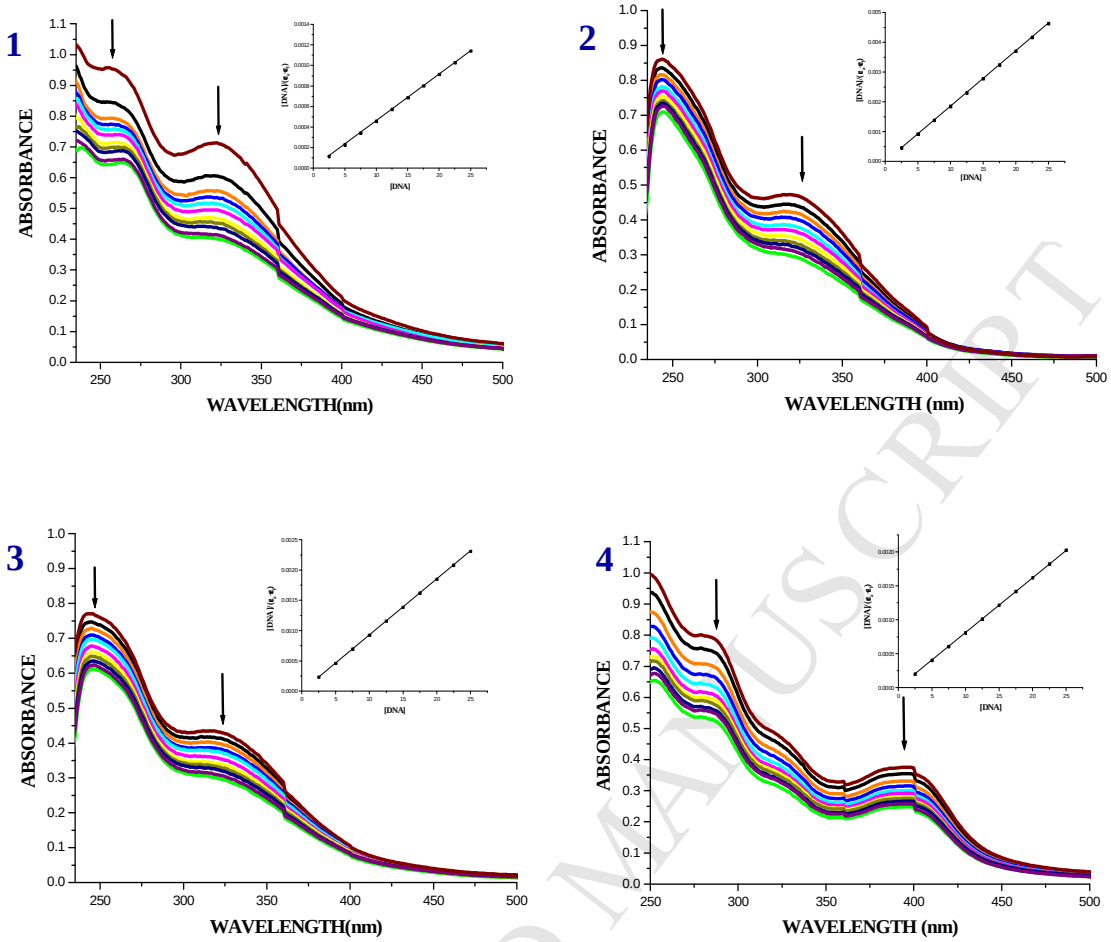

Fig. 6. Absorption titration spectra of complexes (**1-4**) (25 µM) with increasing concentrations (2.5-25 µM) of CT-DNA (Tris HCl buffer, pH 7.2). Inset: Binding isotherms of the complexes **1-4** with CT-DNA

2.3.2. EB-DNA quenching studies

The result obtained from the above experiments suggested that all the complexes can bind with CT-DNA. Further, the binding mode of the complexes with CT-DNA has been confirmed by ethidium bromide (EB) displacement studies. Upon each successive addition of complexes to CT-DNA pretreated with EB ([DNA]/[EB] = 1), a gradual quenching of the fluorescence intensity was observed (Fig. 7). The reduction of the fluorescence emission intensity gives criteria to analyze the DNA binding propensity of the complexes and stacking interaction (intercalation) between the adjacent DNA base pairs [40]. As the concentration of the complexes increased from 10-100 µM, the emission band of DNA-bound EB exhibited quenching up to 26.17, 30.88, 33.98 and 22.99 % of the initial fluorescence intensity together

with a red shift of 2-4 nm for complex **1**, **2**, **3** and **4** respectively. This gives a direct evidence for the intercalative binding mode of the complexes with DNA. The quenching data were calculated by using Stern-Volmer plot and quenching constant is obtained as a slope from the plot of I_o/I_{corr} versus [Q] and are given in Table 3. The data showed that DNA-bound EB can be more readily replaced by the complexes in the order **3** > **2** > **1** > **4**, among the complexes **1-4**, the ligand having terminal ethyl group showed better affinity towards the DNA when compared to the phenyl and methyl group and hydrogen atom in the *N*-terminal position [26]. Further, the calculated K_{SV} values of the compounds are significant when compared to the reported values [26,27,34].

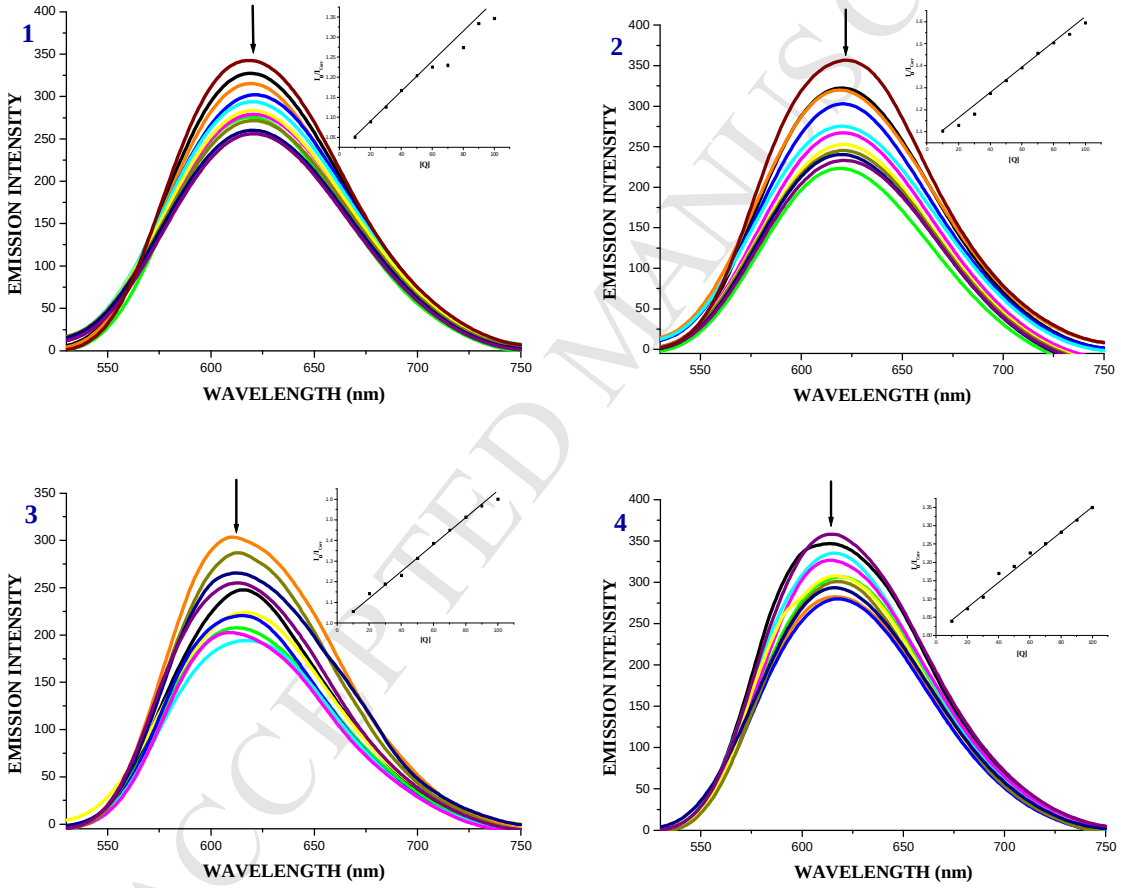

Fig. 7. The emission spectra of the DNA–EB system (λ_{exc}= 515 nm, λ_{em}= 530–750 nm), in the presence of complexs **1-4**. [DNA] = 10 µM, [complex] = 10–100 µM, [EB] = 10 µM. The arrow shows the emission intensity changes upon increasing complex concentration. **Inset**: Stern−Volmer plot of the fluorescence titration of the complexes (**1-4**) (10-100 µM) with DNA-EB (10 µM)

Table 3: The binding constant (K_{bin}) and quenching constant (K_{sv}) values for the interactions of the complexes (**1–4**) with CT-DNA

Compounds	Binding constant K_{bin} M^{-1}	Quenching constant K_{SV} M^{-1}
Complex **1**	7.5280±0.321 x10^5	2.79±0.003 x10^3
Complex **2**	9.2713±0.306 x10^5	3.43±0.006 x10^3
Complex **3**	13.8736±0.320 x10^5	6.19±0.008 x10^3
Complex **4**	6.2265±0.286 x10^5	2.75±0.002 x10^3

2.3.3. Viscosity measurements

In order to confirm the binding mode of the complexes with CT-DNA, viscosity measurements were carried out by keeping the DNA concentration (100 µM) as constant and varying the concentrations of the compounds (20-100 µM). From Fig. 8, it is obvious that the relative viscosity of DNA solutions increased upon increasing the concentration of the complexes. Viscosity of DNA will increase while the complex intercalates between adjacent DNA base pairs, which leads to an increase in the separation of base pairs at the intercalation site, resulting an increase in the overall DNA length [41,42] and the above results concluded that compounds interacted with CT-DNA through an intercalative mode. In addition, from the plot we concluded that the ability of the complexes to increase the viscosity of CT-DNA depends upon the substitution on the *N*-terminal nitrogen of the ligand and the increasing order of viscosity of CT-DNA by the complexes is **(NH-Ethyl) 3** > **(NH-methyl) 2** > **(NH-Hydrogen) 1**> **(NH-Phenyl) 4** which is consistent with their DNA binding results.

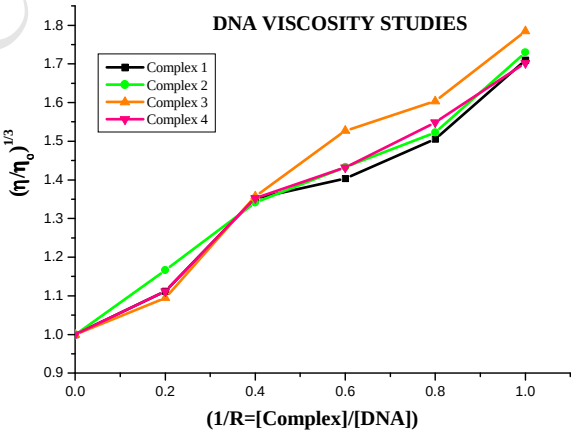

Fig. 8. Effect of the complexes (**1-4**) on viscosity of CT-DNA

2.4. pBR322 DNA cleavage studies

The newly synthesized organoruthenium(II) complexes (**1-4**) were studied for their chemical nuclease activities by the agarose gel electrophoresis method with supercoiled pBR322 DNA as the substrate, in the absence of external agents in a medium of 5 mM Tris-HCl/50 mM NaCl buffer (pH 7.2). The DNA cleavage efficiency was measured by determining the ability of the compound to convert the supercoiled DNA (SC Form) to Linear circular form or nicked form (NC Form). All the four cyclometallated ruthenium(II) complexes efficiently cleaved the supercoiled pBR322 DNA to nicked form and linear circular form (Fig. 9). From Fig. 9 we inferred that the complexes to influence nuclease activity in the order **3** > **2** > **1**≈ **4**, which may be due to the change in the electron donating or accepting ability pertaining to the *N*-terminal substituent of the ligand and subsequent change in the polarisability on metal. Among the complexes, complex **3** with more electron donating ethyl substitution on terminal nitrogen atom causes stronger distortion on DNA strand showing more efficient DNA cleavage. The observed result pattern is parallel to their DNA binding affinity.

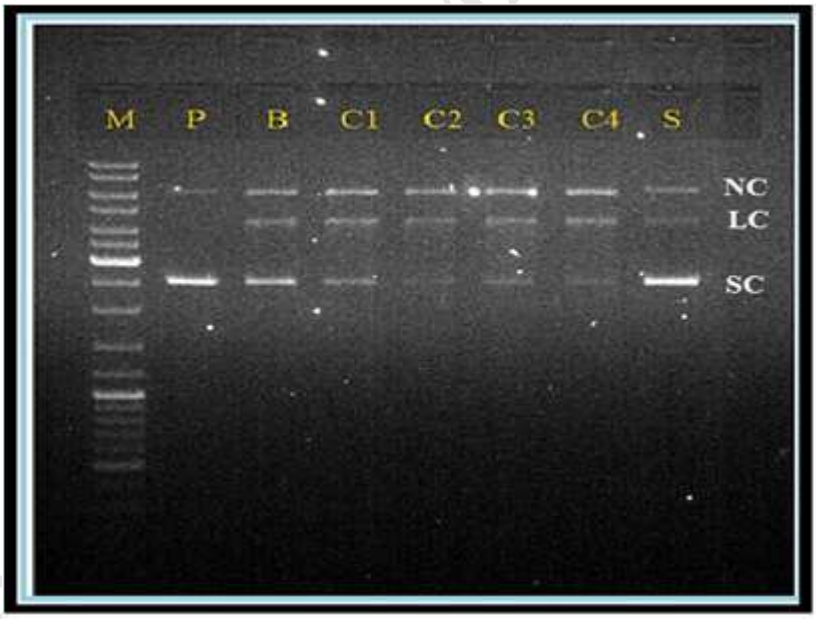

Fig. 9. Gel electrophoresis diagram showing the cleavage of supercoiled pBR322 DNA by complexes **1-4** in 5% DMSO and 95% 5 mM Tris−HCl/50 mM NaCl buffer at pH 7.2 and 37 °C with an incubation time of 2 h. Lanes M: Marker; Lane C 1: Complex **1** (50 µM). Lane C 2: Complex **2** (50 µM); Lane C 3: Complex **3** (50 µM); Lane C 4: Complex **4** (50 µM); Lane S: Metal precursor (50 µM); Forms SC, NC, and LC are supercoiled, nicked circular, and linear circular DNA, respectively.

2.5. Protein Binding Studies

The intrinsic fluorescence of BSA and HSA is mainly due to tryptophan residue [43,44]. The binding of new Ru(II) complexes **1–4** with BSA and its homologue HSA was investigated by fluorescence emission spectroscopy, since the albumin solution exhibits an intense emission band (λ_{ex} = 290 nm) at $\lambda_{em,max}$ = 345 nm (for HSA) and 346 nm (for BSA) which is assigned to the existence of tryptophans. The emission titration studies have been performed at room temperature using BSA (10 μM)/ HSA (10 μM) with increasing concentrations of complexes **1–4** (0−100 μM) in the range 290−500 nm. However, no emission peak appeared around 340-345 nm when these ruthenium complexes were excited with the same excitation wavelength, suggesting that the ruthenium complexes **1-4** would not induce fluorescence interference to serum albumin within the investigated excitation wavelength range. Addition of the above test compounds to BSA solution resulted in a significant decrease in the fluorescence intensity of BSA at 346 nm, up to 63.39, 74.89, 78.71 and 72.34 % of the initial fluorescence intensity of BSA with 2-6 nm blue shift for complexes **1**, **2**, **3** and **4** respectively (Fig. 10). Addition of the compounds to HSA solution resulted in a high quenching of the emission band of HSA at 345 nm up to 51.00, 57.37, 65.91 and 45.62 % of the initial fluorescence intensity together with a blue shift of 2-4 nm for complex **1**, **2**, **3** and **4** respectively (Fig. 11). From the above observations, we may conclude that definite interaction is taking place between the complexes and serum albumins.

Fig. S10 in the supporting information shows the absorption spectra of BSA and HSA in the absence and presence of complexes. The absorbance intensity of serum albumins showed hypochromism with a small blue shift (~ 2-5 nm) in the presence of complexes **1-4**, indicating a static quenching mechanism of the serum albumins by complexes. By using Stern Volmer quenching equation, the values of the Stern Volmer quenching constant (K_{SV}) and the quenching constant (K_q) for complexes interacting with serum albumins (BSA/HSA) were calculated. The Stern Volmer quenching constant obtained as a slope of the plot of [Q] verses the ratio of the fluorescence intensity in the absence (I_o) and in the presence of the quencher (I) (Fig. 12; Table 4) and the results follow the order **3** > **2** > **1** > **4**. The observed Ksv values are comparable to those reported for other ruthenium complexes [20,26,34,38,39]. The quenching constant values ($k_q \approx 10^{12}$ M^{-1} s^{-1}) suggested the good binding affinity of the complexes with serum albumins through static quenching mechanism [45].

The binding constant K_{bin} and number of binding site (n) can be calculated from the Scatchard equation and are given in Table 4 (Fig. 13), from these values we knew that the complexes (**1-4**) showed strong binding affinity with serum albumins. Further, the obtained results suggested that complexes **1-4** act as potent binders with serum albumins. From the results, we confirmed that the Ru(II) complexes having a large hydrophobic area can interact more efficiently with serum albumins via a static pathway. The obtained binding constant and quenching constant values revealed that the ruthenium(II) complexes bind to both the albumins in the following order **3** > **2** > **1** > **4**. This observed trend can be explained on the basis of electron donating ability and hydrophobicity of the compounds. Increase in the electron-donating ability of the *N*-terminal substituent of the coordinated ligand increases the electron density on the electron deficient metal center [46]. As seen from the results, complex **3** with the enhanced hydrophobicity showed the best binding ability [34]. The obtained quenching constant and binding constant values of these new cyclometallated ruthenium(II) complexes agree well with those reported for other ruthenium(II) complexes [20,47,48].

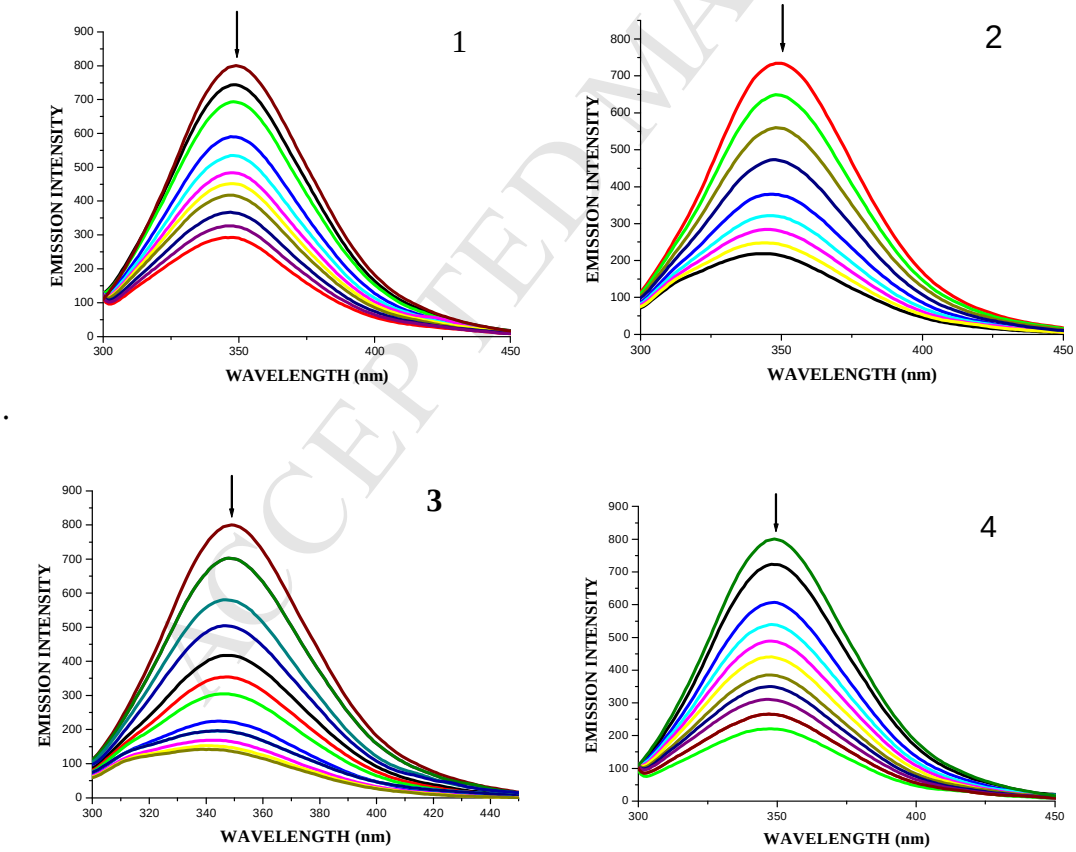

Fig. 10. The emission spectra of BSA (10 µM; λ_{exc}= 280 nm; λ_{emi}= 346 nm) in the presence of increasing amounts of complexes **1-4** (10–100 µM). The arrow shows the emission intensity changes upon increasing complex concentration

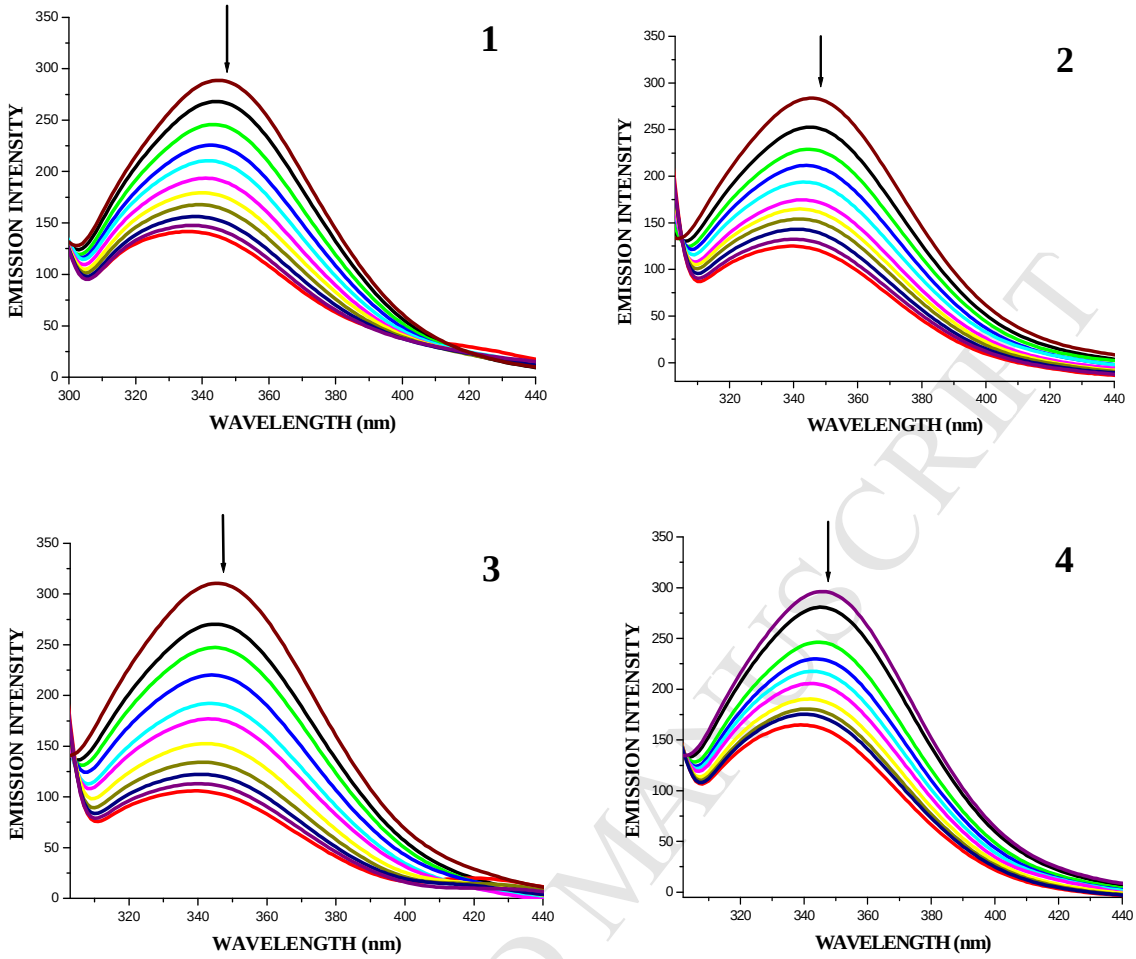

Fig. 11. The emission spectra of HSA (10 µM; λ_{exc}= 280 nm; λ_{emi}= 346 nm) in the presence of increasing amounts of complexes **1-4** (10–100 µM). The arrow shows the emission intensity changes upon increasing complex concentration

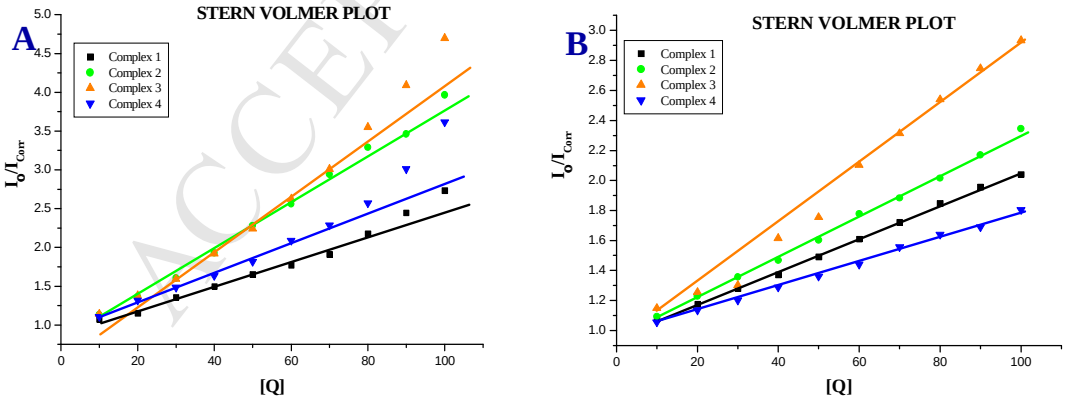

Fig. 12. **A**) Stern−Volmer plot of the fluorescence titration of the complexes (**1-4**) (10-100 µM) with BSA (10 µM). **B**) Stern−Volmer plot of the fluorescence titration of the complexes (**1-4**) (10-100 µM) with HSA (10 µM)

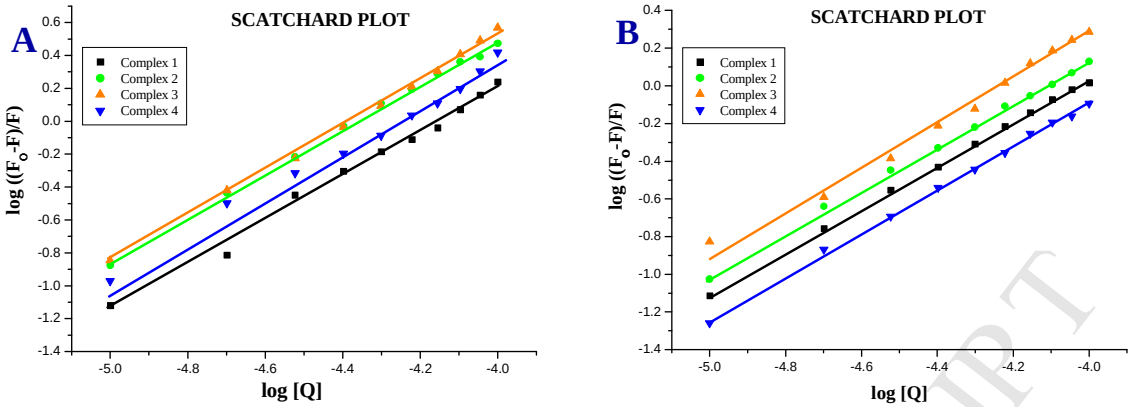

Fig. 13. **A**) Scatchard plot of the fluorescence titration of the complexes (**1-4**) (10-100 µM) with BSA (10 µM). **B**) Scatchard plot of the fluorescence titration of the complexes (**1-4**) (10-100 µM) with HSA (10 µM)

Table 4: Stern volmer quenching constant (K_{sv}), Quenching constant (k_q), binding constant (K_{bin}) and number of binding sites (n) for the interactions of ligands and complexes (1-4) with BSA/HSA

Compounds	Stern-Volmer K_{sv}/M^{-1}	Quenching Constant (k_q) $M^{-1}s^{-1}$	Binding constant K_{bin}/M^{-1}	n
BSA				
Complex **1**	$1.784\pm0.090\times10^{4}$	$1.784\pm0.090\times10^{12}$	$4.363\pm0.182\times10^{5}$	1.3569±0.041
Complex **2**	$3.147\pm0.012\times10^{4}$	$3.147\pm0.012\times10^{12}$	$6.914\pm0.088\times10^{5}$	1.3384±0.020
Complex **3**	$3.904\pm0.033\times10^{4}$	$3.904\pm0.033\times10^{12}$	$1.361\pm0.105\times10^{6}$	1.3996±0.024
Complex **4**	$2.552\pm0.002\times10^{4}$	$2.552\pm0.002\times10^{12}$	$3.490\pm0.043\times10^{5}$	1.2991±0.045
HSA				
Complex **1**	$1.100\pm0.012\times10^{4}$	$1.100\pm0.012\times10^{12}$	$3.808\pm0.039\times10^{4}$	1.1371±0.009
Complex **2**	$1.367\pm0.021\times10^{4}$	$1.367\pm0.021\times10^{12}$	$4.460\pm0.014\times10^{4}$	1.1306±0.015
Complex **3**	$2.091\pm0.067\times10^{4}$	$2.091\pm0.067\times10^{12}$	$9.131\pm0.041\times10^{4}$	1.1716±0.043
Complex **4**	$0.830\pm0.015\times10^{4}$	$0.830\pm0.015\times10^{12}$	$3.212\pm0.015\times10^{4}$	1.1493±0.015

2.5.1. Conformational Investigation

Synchronous fluorescence experiments have been performed to determine the conformational changes in serum albumins such as BSA and HSA in the presence of compounds. In the synchronous fluorescence spectra of the tyrosine residue of both the serum albumins, the addition of the compounds to the solution of BSA/HSA showed hypochromism with negligible shift in the emission wavelength (Fig. S11-S12). Synchronous fluorescence spectra of BSA at $\Delta\lambda$ = 60 nm exhibited a decrease in fluorescence intensity up to 70.69-78.04 % at 340 nm with significant blue shift for complexes (**1-4**) (Fig. S13), whereas the spectra corresponding to the tryptophan residue of HSA, the addition of the compounds to the solution of HSA showed hypochromism upto 43.96-62.51 % for complexes (**1-4**) (Fig. S14). The obtained results clearly revealed that compounds effectively bind with serum albumins and affect the conformation of the tryptophan and tyrosine micro regions.

2.5.2. Three-dimensional fluorescence spectra analysis

Three dimensional fluorescence spectroscopic studies have been performed to investigate the microenvironmental changes in BSA/HSA during interaction with the compounds. Fig. 14-15 shows the three dimensional emission spectra and contour ones of serum albumins in the absence and presence of ruthenium(II) complexes and their corresponding characteristic parameters are provided in Table S2. The emission intensity of peak ‘A’ corresponding to the Rayleigh first order scattering peak increased upon adding the complexes to serum albumins. This is due to the compound formation of serum albumins with our ruthenium(II) complexes leading to an increase in the diameter of the macromolecule which in turn resulted in the enhancement of scattering effect [49]. The fluorescence intensity of peak ‘B’ corresponding to the tryptophan and tyrosine residues decreased with slight blue shift. The obtained results inferred that the molecular conformational and microenvironment changes of protein occurred after interaction with the complexes.

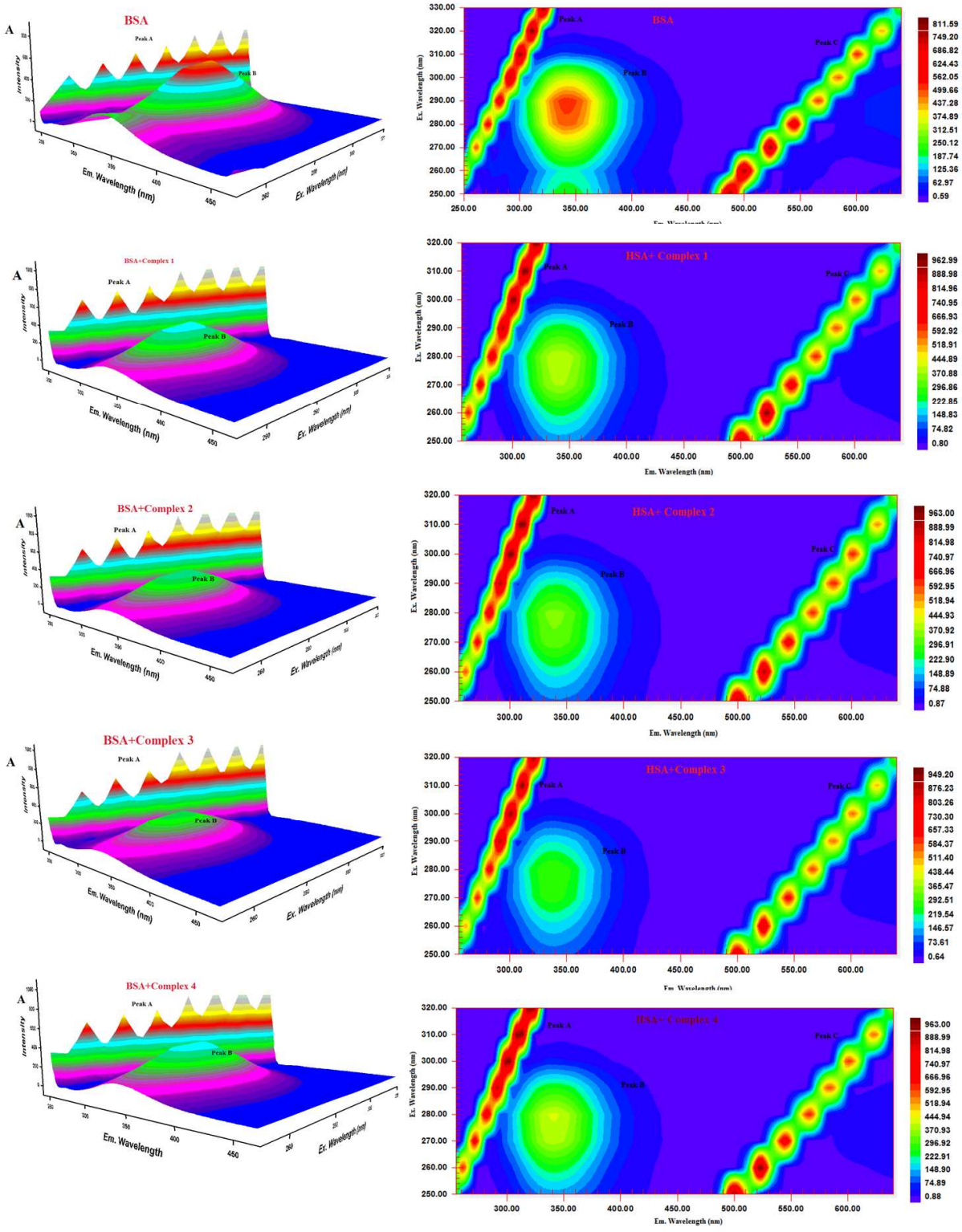

Fig. 14. Three-dimensional fluorescence spectra of BSA in the absence and presence of ruthenium(II) complexes **1-4** (pH 7.4, 298 K, [BSA] =10 μM, [Complex] =10 μM)

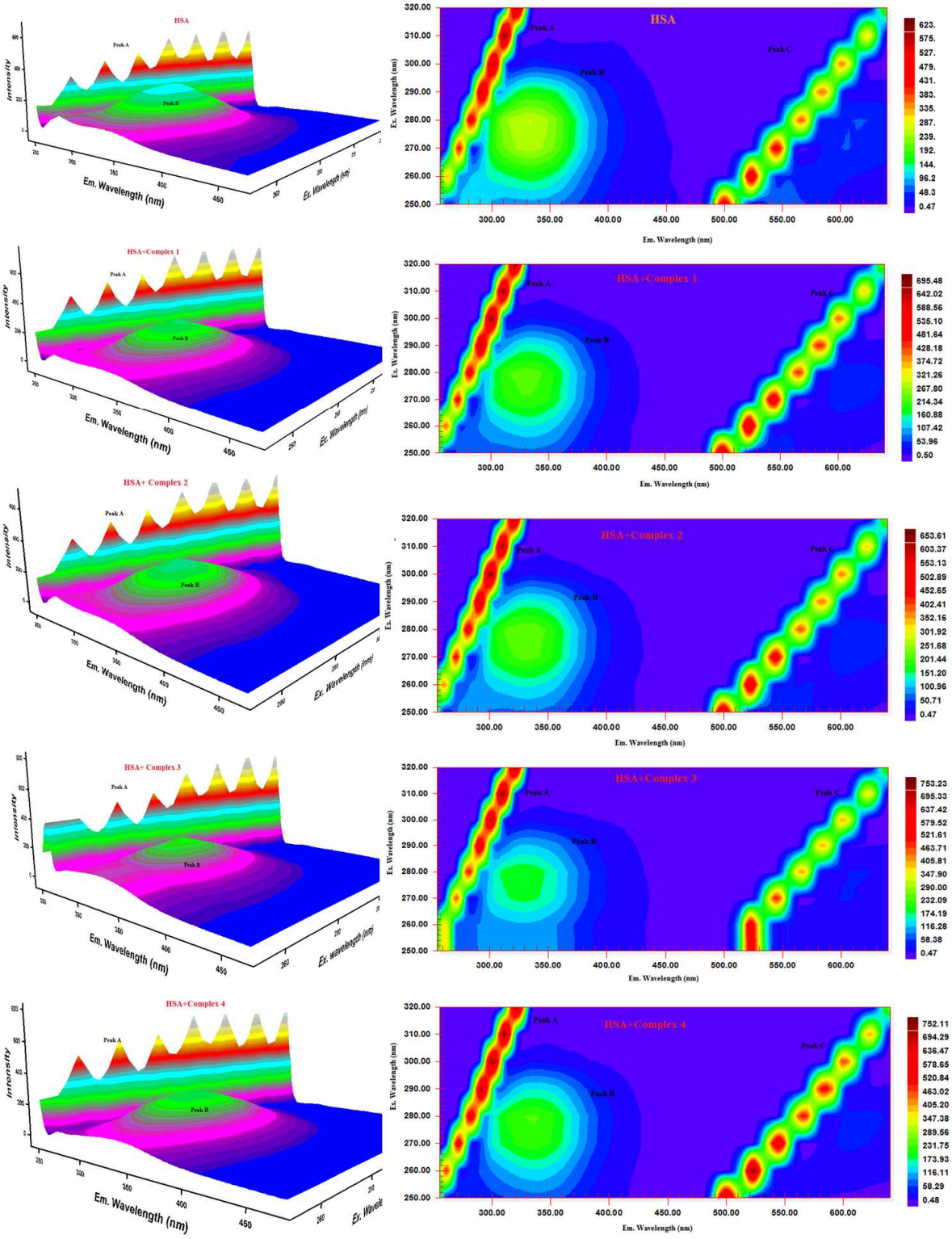

Fig. 15. Three-dimensional fluorescence spectra of HSA in the absence and presence of ruthenium(II) complexes **1-4** (pH 7.4, 298 K, [HSA] =10 μM, [Complex] =10 μM)

2.6. *In vitro* Antioxidant activity

The compounds which exhibit radical scavenging activity are receiving much attention because they possess interesting anticancer, anti-inflammatory and anti-ageing activities [50]. The analysis of the DPPH radical scavenging ability of cyclometallated Ru(II) complexes have been carried out along with the standard Vitamin C. The results showed that the activity of the compounds is higher than that of the standard, the DPPH scavenging activity of the Ru(II) complexes (8.23-9.85 μM) follow the order of **3** > **2** > **1** > **4** (Fig. 16 and Fig. S15). Complex **3** shows the best DPPH scavenging activity among the complexes. The phosphomolybdenum assay is quantitative, since the antioxidant activity is expressed as the number of equivalents of ascorbic acid (Table 5). Four new cyclometallated Ru(II) complexes exhibited higher activity than their parent ligands among them complex **3** contains the more electron donating ethyl substitution at terminal nitrogen showed higher activity. A comparison of the radical scavenging activity of Ru(II) complexes **1–4** with that of the reported Ru(II) Schiff base complexes may reveal that our new Ru(II) complexes **1–4** act as potent radical scavengers [51].

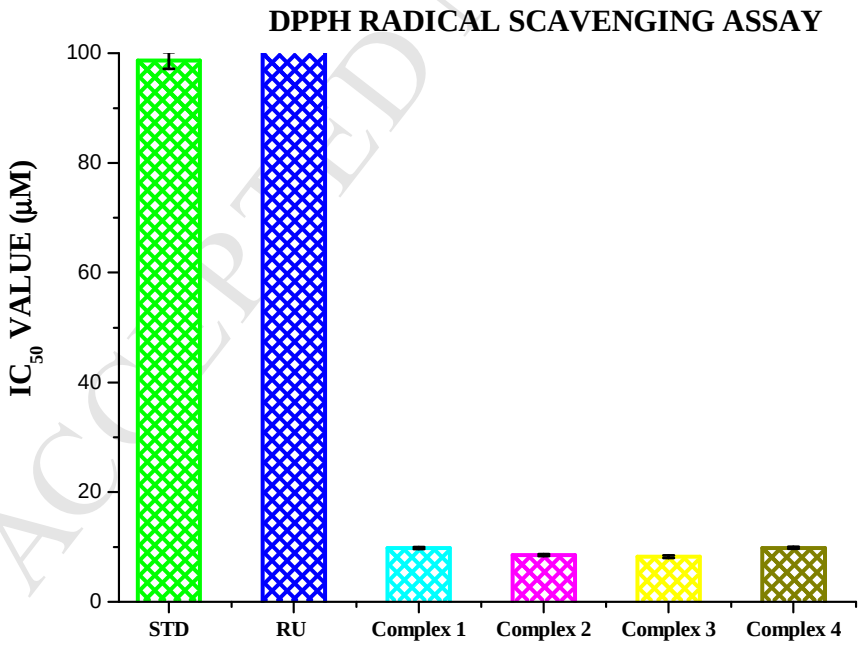

Fig.16. The DPPH radical scavenging activity of the [RuHCl(CO)(PPh_3)$_3$] and new Ru(II) complexes (**1-4**)

Table 5: Estimation of Total antioxidant capacity of [RuHCl(CO)(PPh_3)$_3$] and new Ru(II) complexes (**1-4**)

Compounds	µg Ascorbic acid equivalents/ml
[RuHClCO(PPh_3)$_3$]	07.02±0.08
Complex **1**	50.03±0.73
Complex **2**	59.16±0.65
Complex **3**	63.38±0.89
Complex **4**	49.33±0.54

2.7. Antimicrobial activity

In vitro antimicrobial activities of four new complexes **1–4** were investigated with few pathogenic bacteria such as *Pseudomonas aeruginosa*, *Streptococcus pneumonie*, *Staphylococcus aureus*, *Salmonella paratyphi* and with few fungi *Candida albicans*, *Aspergillus niger*, *Trichophyton rubrumi*, *Candida tropicalis* and *Aspergillus fumigatus*. The results are expressed as the zone of inhibition and minimum inhibitory concentration (MIC) and the effect of the compounds was susceptible to their concentration used for inhibition (Table S3-S6). For comparison, MIC values for positive control such as Gentamicin for bacteria and Ketaconazole for fungi are also given. On comparing the activity of the complexes, complex **3** was more active on bacteria namely *S. aureus*, *S. pneumonie* and *P. aeruginosa*. When tested against *S. paratyphi*, both the complexes **1** and **3** showed comparable activity. Complex **3** was much more efficient in inhibiting the growth of fungal species like *T. rubrum* (IC_{50} = 16.93±0.31 µM), *A. fumigatus* (IC_{50} = 15.78±0.18 µM) and *C. albicans* (IC_{50} = 14.43±0.17 µM), whereas complex **1** was the most active against *A. niger*. Complexes **1** and **3** were approximately equally active over *C. tropicalis*. All the compounds showed lower activity than the controls used. Overall, complex **3** was the better candidate for the growth inhibition of the microorganisms. The complexes showed different degrees of antimicrobial activity due to the structural variations of themselves and variation on the group of microorganisms [52]. Tested complexes had better antimicrobial activity than the ligands against all pathogens. This may be explained by Tweedy's chelation theory [53], which stated that, upon complexation the polarity of metal ion gets reduced which increases the lipophilicity of the metal complexes facilitating them to cross the cell membrane easily [53,54]. The antimicrobial activity against the control disc with 10% aqueous DMSO showed no zone of inhibition. In addition, antimicrobial activity of the complexes was compared with

already reported ruthenium complexes, showing that the new Ru(II) complexes exhibited significant activity [26,55].

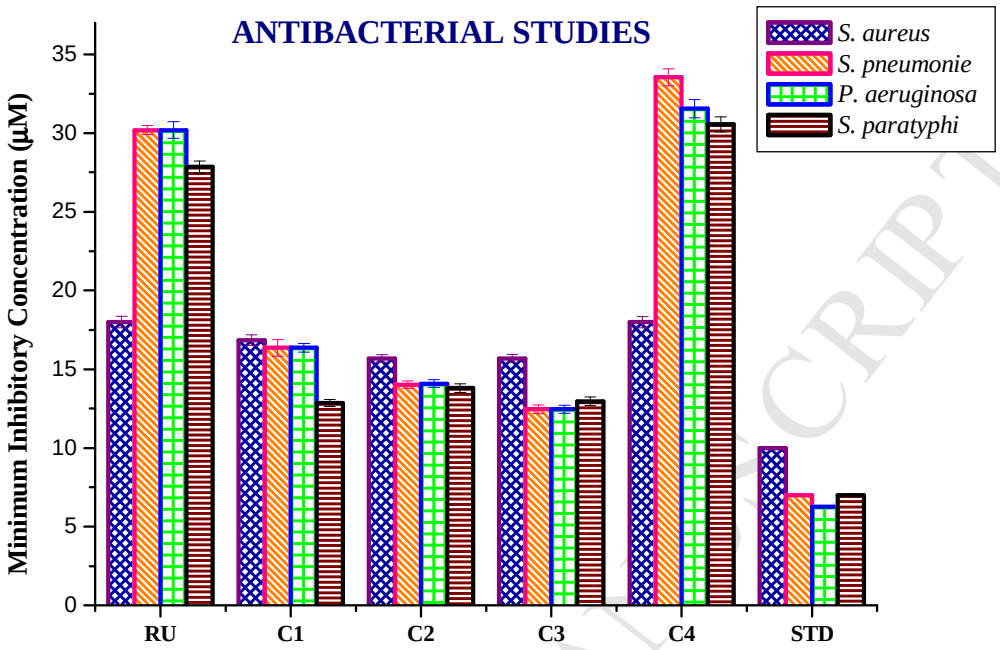

Fig. 17. Anti bacterial activity of [RuHClCO(PPh_3)$_3$] and new Ru(II) complexes (**1-4**). Error bars represent the standard deviation of the mean (n=3)

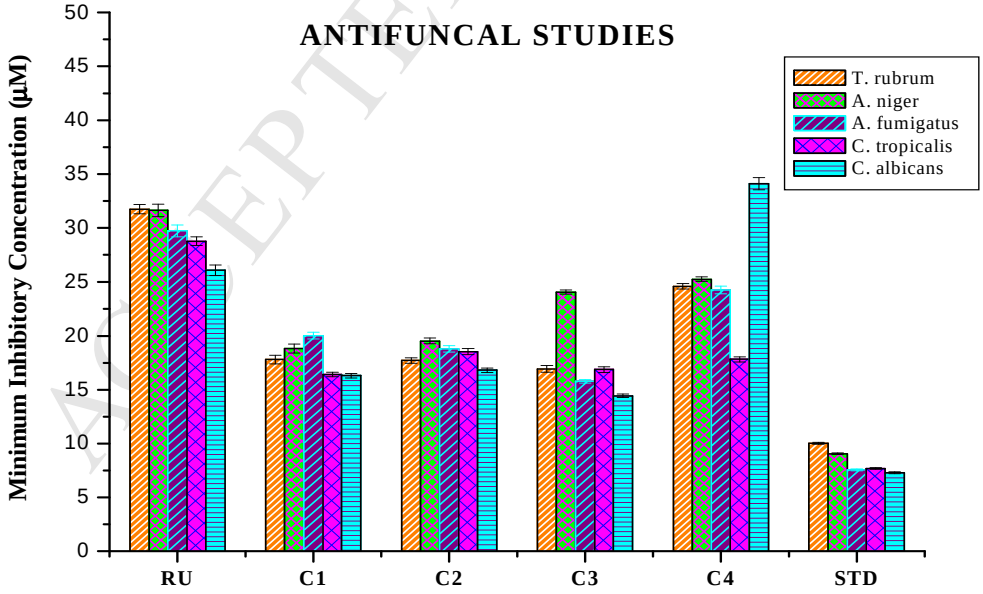

Fig. 18. Anti fungal activity of [RuHClCO(PPh_3)$_3$] and new Ru(II) complexes (**1-4**). Error bars represent the standard deviation of the mean (n=3)

2.8. Cytotoxicity studies

2.8.1. Antiproliferative Studies - Cancer Cell Growth Inhibition

Significant results obtained from DNA/protein binding, antioxidant and antimicrobial studies motivated us to further explore their antiproliferative activities. The compounds were subjected to study the *in vitro* cytotoxicity by MTT assay towards following three cell lines: human lung cancer cells (A549), human breast cancer cells (MCF-7) and human normal keratinocyte cell lines (HaCaT). Cytotoxic activity of *cisplatin* against all the above cell lines was investigated under the same experimental conditions for comparison purposes. The anticancer activity was assessed on the basis of IC_{50} values (the concentration of a drug required to inhibit the growth of 50% of the cells) and the obtained values of the complexes against selected three tumor cell lines are shown in Table 7. The results revealed that Ru(II) complexes exhibited potent antitumor activities than their parent ligands and standard drug *cisplatin* against the selected cell lines in different concentrations and the antitumor activities are concentration-dependent (Fig. S16 - S18). In human breast cancer cell lines (MCF-7), the anticancer activity of the complexes follows the order *cisplatin* (16.79±0.08) < complex **4** (3.93±0.08) < complex **1** (3.86±0.11) < complex **2** (3.77±0.09) < complex **3** (3.72±0.11). The cytotoxic nature of the compounds against human lung cancer cell lines (A549) is in the order *cisplatin* (15.10±0.05) < complex **4** (4.31±0.08) < complex **1** (4.12±0.11) < complex **2** (3.93±0.13) < complex **3** (3.81±0.10).

From the results we knew that cyclometallated Ru(II) complexes (**1-4**) appeared to be more cytotoxic against A549 and MCF-7 cells over their parent ligands. On the basis of the results, the antiproliferative activity of the complexes has been arranged in the order **3** > **2** > **1** > **4**. The observed trend may be due to the presence of different substituents in the terminal nitrogen atom of the ligands. The anticancer activity of the complexes increased with increase in the electron donating ability of the substituent on the terminal nitrogen of the coordinated thiosemicarbazones. It is notable that complex **3** having more electron donating ethyl group at terminal nitrogen has a high antiproliferative activity, as compared with remaining complexes against both the cell lines (MCF-7 and A549) and its IC_{50} value which is almost five times greater than that of *cisplatin* indicated its high cytotoxic effects against human cancer cells. Interestingly, this observed trend is in agreement with their previous biological studies, suggesting that the anticancer activities of the tested compounds against cancer cell lines may be related to their ability to intercalate the base pairs of the DNA and/or their free radical scavenging activity. The compounds were also screened for their activity on

the human normal keratinocyte cells (HaCaT) to examine the selectivity of the compounds for cancer cells rather than normal cell lines and the results inferred that the complexes are significantly non toxic to normal cells. The anticancer activity of our new cyclometallated Ru(II) complexess are superior to those reported some other Ru(II) Schiff base complexes against A549 cell lines and MCF-7 cells [14,20,21,24,27,56-59].

Table 7. The IC_{50} values for the human breast cancer cell line MCF-7, human lung carcinoma cancer cell line A549 and human normal keratinocyte cells (HaCaT) with new organometallic Ru(II) complexes for 48h

Compounds	IC_{50} values (μM)		
	MCF-7	A549	HaCaT
Cisplatin	16.79±0.08	15.10±0.05	>40
$[RuHClCO(PPh_3)_3]$	20.10±0.18	15.96±0.21	>40
Complex **1**	3.96±0.11	4.12±0.11	>40
Complex **2**	3.74±0.09	3.93±0.13	>40
Complex **3**	3.72±0.11	3.81±0.10	>40
Complex **4**	3.85±0.08	4.31±0.08	>40

2.8.2. LDH assay

To further evaluate the toxicity of the compounds, activity of LDH was measured. LDH is a stable cytoplasmic enzyme released into the culture medium due to the loss of membrane integrity resulting from apoptosis of cells. Hence, LDH release is used to analyse drug induced cytotoxicity of cancer cells [60]. When cancer cell lines A549 and MCF-7 were treated with the IC_{50} concentration of the new cyclometallated ruthenium(II) complexes **1-4** for a period of 48 h, a significant increase of LDH release in the culture medium was observed (Fig. 19). These results indicated the efficiency of the complexes in inducing cell death by collapsing the membrane integrity. The complexes showed good level of LDH leakage in A549 and MCF-7 cells compared to *cisplatin*. This study authenticate that complex **3** was more effective followed by complex **2**, **1** and **4**. The ruthenium(II) complexes showed significant activity when compared with the earlier reports [34].

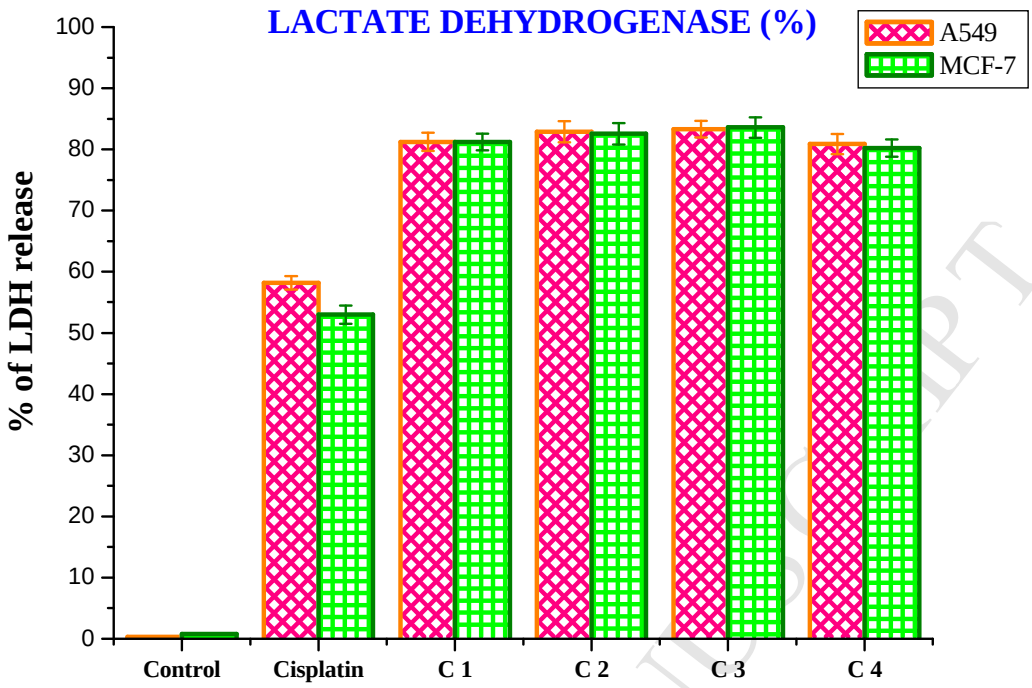

Fig. 19. Percentage of lactate dehydrogenase released by the human cancer cell lines A549 and MCF-7 after an incubation period of 48 h with complexes **1-4**. Error bars represent the standard mean error (n= 6).

2.8.3. Nitric oxide assay

The nitric oxide (NO) assay is also an important measure of cytotoxicity, as NO has been shown to directly inhibit methionine adenosyl transferase, leading to glutathione depletion, and its reaction with superoxide generates the strong oxidant peroxynitrite, which can initiate lipid peroxidation or cause a direct inhibition of the mitochondrial respiratory chain [61]. In the present study NO release by the new ruthenium(II) complexes **1-4** was evaluated using A549 and MCF-7 cells. The quantification of the nitrite produced in the cell media by the Griess assay is an indirect but cost-effective measurement of the amount of NO produced by the cells. It is interesting to note that the complexes were found to release more NO than the *cisplatin* and control (Fig. 20). In addition, complex **3** was more effective in enhancing the level of NO in the culture medium and the activity follows the order **3** > **2** > **1** > **4** and hence the results confirmed the cytotoxic potential of the studied compounds.

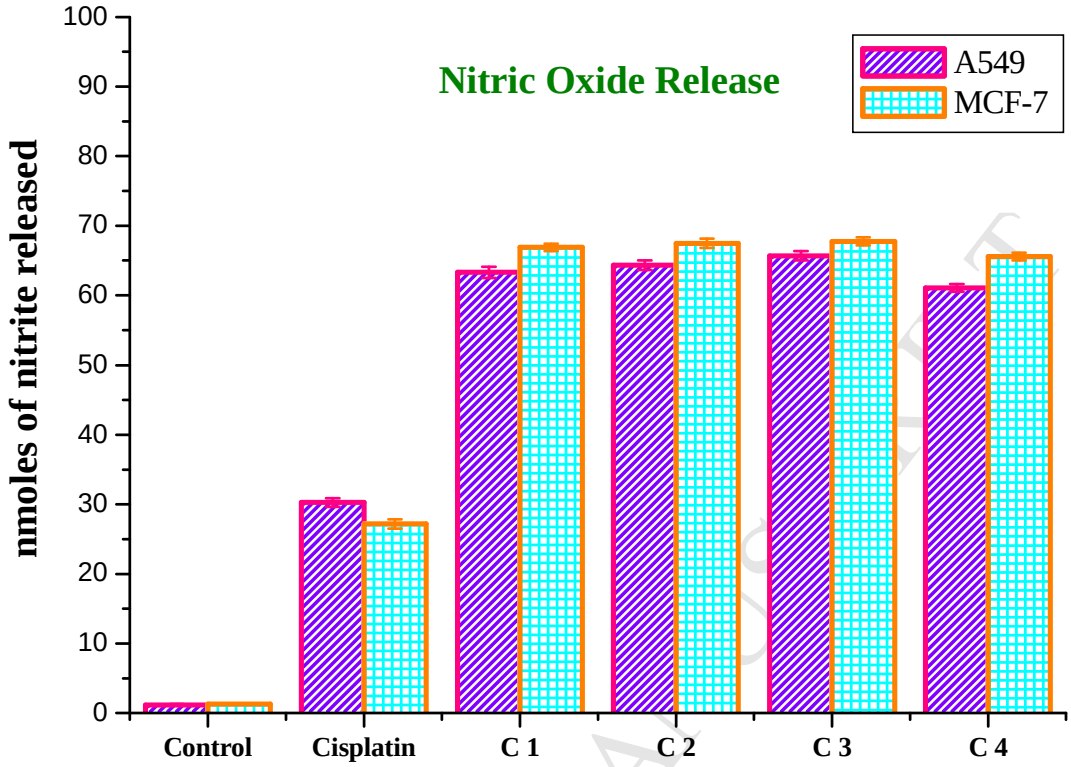

Fig. 20. Nitrite released (nmoles) by the human cancer cell lines A549 and MCF-7 after an incubation period of 48 h with complexes **1-4**. Error bars represent the standard mean error (n= 6).

3. Conclusion

New potential anticancer active cyclometallated Ru(II) complexes (**1-4**) were synthesized by the complexation of 3-acetyl-8-methoxycoumarin-4*N*-substituted thiosemicarbazones with $[RuHCl(CO)(PPh_3)_3]$. Elemental analyses and spectroscopic characterizations (IR, UV-Vis, ^{1}H NMR and ^{13}C NMR) supported the formation of the complexes. The crystal structures of the complexes **1**, **2** and **4** have been solved by X-ray crystallographic analysis. Intercalative binding mode of the compounds with CT-DNA was suggested by the spectral, EB displacement assay and DNA viscosity measurements. The compounds were able to bind well with BSA/HSA and a static quenching mechanism was observed. 3D fluorescence experiments indicated the changes in the protein microenvironment. The compounds have good radical scavenging property and antimicrobial studies revealed the significant activity of the compounds. The complexes were better in damaging cancerous cell lines than the *cisplatin*. They were found to be non toxic against

human normal keratinocyte cell line HaCaT. Combining the overall results, it is evident that the biological activity of the complexes follows the pattern **3** > **2** > **1** > **4** and the promising results obtained from the biological studies suggested that the complexes can act as good probes for further exposure in pharmaceutical applications..

4. Experimental section

4.1. Materials and methods

All the reagents used were of analytical or chemically pure grade. Solvents were purified and dried according to standard procedures [62]. 3-acetyl-8-methoxy-2H-chromen-2-one [63] and the metal precursor $[RuHCl(CO)(PPh_3)_3]$ were prepared according to the literature procedures [64]. The 3-acetyl-8-methoxy-2H-chromen-2-one-4(N)-substituted thiosemicarbazones $\mathbf{H_2L^{1\text{-}4}}$ were prepared with a slight modification of the reported method [37,63]. Buffers were prepared from doubly distilled water. Ethidium bromide (EB), bovine serum albumin (BSA), calf thymus DNA (CT-DNA) and 3-(4,5-dimethylthiazol-2-yl)-2,5-diphenyltetrazolium bromide (MTT) were purchased from HiMedia and used as received. Melting points were measured in a Lab India apparatus. Infrared spectra were measured as KBr pellets on a JASCO FT-IR 4100 instrument between 400–4000 cm^{-1}. Elemental analyses of carbon, hydrogen, nitrogen and sulfur was determined by using Vario EL-III CHNS analyser. The electronic spectra of the complexes were recorded with a JASCO V-630 spectrophotometer using DMSO as the solvent in the 800–200 nm range. Emission spectra were recorded by using JASCO FP 6600 Spectrofluorimeter. ^1H and ^{13}C NMR spectra of the compounds were recorded in DMSO with a Bruker instrument with 400 MHz and 100 MHz respectively, chemical shift relative to tetramethylsilane.

4.2. X-ray Crystallography

Suitable single crystals for the complexes (**1, 2** and **4)** were obtained from dichloromethane/methanol medium. Single crystal data collections and corrections for the new Ru(II) complexes (**1**, **2** and **4**) were carried out with a Bruker kappa APEX-II DUO 1000 CCD diffractometer using graphite monochromated Mo Kα (λ= 0.71073 Å) radiation at 90.05 K. All the calculations were done by using SHELXS-97 [65] and SHELXL-2014/7 programs [66].

4.3. General procedure for the synthesis of new ruthenium(II) complexes [Ru(8MAC-Rtsc)(CO)(PPh_3)$_2$]

A solution of 3-acetyl-8-methoxy-coumarin thiosemicarbazone/ 3-acetyl-8-methoxy-coumarin-4(*N*)-methylthiosemicarbazone/3-acetyl-8-methoxy-coumarin-4(*N*)-ethylthiosemi carbazone / 3-acetyl-8-methoxy-coumarin-4(*N*)-phenylthiosemicarbazone (0.105 mmol) in 10 cm^3 of benzene was added dropwise to a boiling solution of [RuHCl(CO)(PPh_3)$_3$] (0.105 mmol) in benzene and refluxed for 7 h and allowed to stand for 4 days at room temperature. Reddish orange solid formed was filtered, washed with petroleum ether (60–80 °C) and recrystallized from dichloromethane and methanol mixture (1:1 v/v).

4.3.1. Synthesis of [Ru(8MAC-tsc)(CO)(PPh_3)$_2$] (1)

Yield: 68 %. Mp. 163 °C. Anal. calcd. for $C_{50}H_{41}N_3O_4P_2RuS$: C, 63.67; H, 4.39; N, 4.45; S, 3.39. Found: C, 63.59; H, 4.30; N, 4.40; S, 3.35 %. FT-IR (ν, cm^{-1}) in KBr: ν(C=O lactone) 1687, ν(C=N) 1590, ν(C-S) 729, ν(C≡O) 1914, 1434, 1089, 695 (for PPh_3). UV-Vis (DMSO), λ_{max} (ε): 267 (15,252) nm ($dm^3mol^{-1}cm^{-1}$) (Intraligand transition); 324 (16,786) nm ($dm^3mol^{-1}cm^{-1}$) (LMCT s→d). ^{1}H NMR (400 MHz, DMSO-d_6, δ ppm, *J* Hz): δ 7.15-7.31 (m, 31H, Ar-H), δ 6.62-6.66 (t, 1H, *J*=7.2, C6-H), δ 6.91-6.93 (d, 1H, *J*=8, C7-H), δ 3.79 (s, 3H,-OCH_3), δ 2.09 (s, 3H,-CH_3), δ 5.74 (br s, 2H, -NH_2). ^{13}C NMR (100 MHz, DMSO-d_6, δ ppm): δ 201.4 (C≡O), δ 162.9 (C-S), δ 161.9 (C=N), δ 151.2 (C=O), δ 112.6 (C2), δ 145.7 (C3), δ 126.3 (C4), δ 121.4 (C5), δ 125.5 (C6), δ 121.1 (C7), δ 139.1 (C8), δ 127.9 (C9), δ 18.2 (-CH_3), δ 56.1 (OMe), δ 128.6-133.3 (PPh_3). Complex **1** was recrystallized from dichloromethane and methanol mixture (1:1 v/v) to yield red transparent, needle like crystals suitable for X-ray analysis.

4.3.2. Synthesis of [Ru(8MAC-mtsc)(CO)(PPh_3)$_2$] (2)

Yield: 62%. Mp. 206 °C. Anal. calcd. for $C_{51}H_{43}N_3O_4P_2RuS$: C, 64.00; H, 4.45; N, 4.39; S, 3.34. Found: C, 63.63; H, 4.49; N, 4.34; S, 3.30 %. FT-IR (ν, cm^{-1}) in KBr: ν(C=O lactone) 1682, ν(C=N) 1592, ν(C-S) 745, ν(C≡O) 1930, 1407, 1089, 696 (for PPh_3). UV-Vis (DMSO), λ_{max} (ε): 244 (86,054) nm ($dm^3mol^{-1}cm^{-1}$) (Intraligand transition); 318 (47,292) nm ($dm^3mol^{-1}cm^{-1}$) (LMCT s→d), 531 (1057) nm ($dm^3mol^{-1}cm^{-1}$) (forbidden d→d transition). ^{1}H NMR (400 MHz, DMSO-d_6, δ ppm, *J* Hz): δ 7.13-7.30 (m, 31H, Ar-H), δ 6.74-6.78 (t, 1H, *J*=7.6, C6-H), δ 6.85-6.87 (d, 1H, *J*=7.2, C7-H), δ 3.89 (s, 3H,-OCH_3), δ 2.09 (s, 3H,-CH_3), δ 6.09-6.29 (q, 1H, terminal -NH), δ 2.10-2.11 (d, 3H, *J*=4.8,-NH-CH_3). ^{13}C NMR (100

MHz, DMSO-d_6, δ ppm): δ 193.6 (C≡O), δ 163.2 (C-S), δ 162.6 (C=N), δ 150.1 (C=O), δ 112.5 (C2), δ 145.7 (C3), δ 126.3 (C4), δ 121.6 (C5), δ 126.3 (C6), δ 121.1 (C7), δ 139.1 (C8), δ 137.6 (C9), δ 18.1 (-CH_3), δ 56.1 (OMe), δ 22.0 (-NH-CH_3), δ 127.4-133.6 (PPh_3). Needle shaped, transparent red colour crystals were obtained by recrystallization of complex **2** in dichloromethane and methanol mixture.

4.3.3. Synthesis of [Ru(8MAC-etsc)(CO)(PPh_3)$_2$] (3)

Yield: 66 %. Mp.146 °C. Anal. calcd. for $C_{52}H_{45}N_3O_4P_2RuS$: C, 64.31; H, 4.68; N, 4.32; S, 3.30. Found: C, 63.25; H, 4.60; N, 4.27; S, 3.26 %. FT-IR (ν, cm^{-1}) in KBr: ν(C=O lactone) 1687, ν(C=N) 1590, ν(C-S) 752, ν(C≡O) 1938, 1434, 1090, 696 (for PPh_3). UV-Vis (DMSO), λ_{max} (ε): 245 (77,054) nm ($dm^3mol^{-1}cm^{-1}$) (Intraligand transition); 318 (43,524) nm ($dm^3mol^{-1}cm^{-1}$) (LMCT s→d). ^{1}H NMR (400 MHz, DMSO-d_6, δ ppm, *J* Hz): δ 7.13-7.63 (m, 31H, Ar-H), δ 6.72-6.75 (t, 1H, *J*=7.2, C6-H), δ 6.89-6.91 (d, 1H, *J*=7.6, C7-H), δ 3.77 (s, 3H,-OCH_3), δ 1.88 (s, 3H,-CH_3), δ 6.39-6.68 (t, 1H, terminal -NH), δ 2.21-2.36 (m, 2H, *J*=4.8,-NH-CH_2), δ 0.70-0.73 (t, 3H, *J*=7.2,-CH_2-CH_3). ^{13}C NMR (100 MHz, DMSO-d_6, δ ppm): δ 203.4 (C≡O), δ 165.8 (C-S), δ 163.2 (C=N), δ 153.1 (C=O), δ 112.4 (C2), δ 145.7 (C3), δ 129.5 (C4), δ 127.4 (C5), δ 127.9 (C6), δ 121.1 (C7), δ 139.5 (C8), δ 130.5 (C9), δ 18.0 (-CH_3), δ 56.1 (OMe), δ 31.1 (-NH-CH_2), 22.0 (terminal -CH_3), δ 128.3-133.6 (PPh_3).

4.3.4. Synthesis of [Ru(8MAC-ptsc)(CO)(PPh_3)$_2$] (4)

Yield: 67%. Mp. 193 °C. Anal. calcd. for $C_{56}H_{45}N_3O_4P_2RuS$: C, 65.99; H, 4.45; N, 4.12; S, 3.14. Found: C, 65.01; H, 4.37; N, 4.05; S, 3.09 %. FT-IR (ν, cm^{-1}) in KBr: ν(C=O lactone) 1682, ν(C=N) 1598, ν(C-S) 743, ν(C≡O) 1921, 1432, 1089, 694 (for PPh_3). UV-Vis (DMSO), λ_{max} (ε): 250 (99,515) nm ($dm^3mol^{-1}cm^{-1}$) (Intraligand transition); 279 (80,102) nm ($dm^3mol^{-1}cm^{-1}$) (Intraligand transition); 397 (37,552) nm ($dm^3mol^{-1}cm^{-1}$) (LMCT s→d). ^{1}H NMR (400 MHz, DMSO-d_6, δ ppm, *J* Hz): δ 6.96-7.34 (m, 36H, Ar-H), δ 6.69-6.78 (m, 2H, C6-H and C7-H), δ 3.80 (s, 3H,-OCH_3), δ 1.99 (s, 3H,-CH_3), δ 8.49 (s, 1H, terminal -NH). ^{13}C NMR (100 MHz, DMSO-d_6, δ ppm): δ 208.6 (C≡O), δ 166.4 (C-S), δ 166.0 (C=N), δ 153.1 (C=O), δ 112.9 (C2), δ 145.8 (C3), δ 1296.4 (C4), δ 120.2 (C5), δ 121.3 (C6), δ 118.5 (C7), δ 141.3 (C8), δ 139.2 (C9), δ 18.6 (-CH_3), δ 56.1 (OMe), δ 127.5-133.4 (PPh_3). Single crystals suitable for X-ray diffraction studies were obtained by recrystallisation of complex **4** in dichloromethane and methanol solution.

4.4. Biomolecular interaction studies

The stability of the complexes was performed in 1 % aqueous DMSO, phosphate buffer–DMSO (99:1) and Tris-HCl–DMSO (99:1). The stability was analyzed by monitoring the electronic spectra over 24 h at room temperature on a JASCO 4100 spectrophotometer. DNA binding studies, DNA viscosity studies, DNA cleavage experiments and protein binding studies have been carried out according to the method described in our earlier reports [26,34,59].

4.5. *In vitro* antioxidant assays

The DPPH radical scavenging assay of the compounds has been done according to the reported method [67]. In this study, various concentrations of the experimental standard ascorbic acid, $[RuHCl(CO)(PPh_3)_3]$ (20-100 µM) and complexes (2-10 µM) in methanol were taken. Total antioxidant activity of the compounds was determined by the phosphomolybdate method [68].

4.6. *In vitro* antimicrobial assay

Antimicrobial activities of the compounds were evaluated by agar well diffusion method [69] as reported, by taking *Staphylococcus aureus*, *Streptococcus pneumonie*, *Pseudomonas aeruginosa*, *Salmonella paratyphi* and fungus such as *Candida albicans*, *Trichophyton rubrum*, *Aspergillus niger*, *Aspergillus fumigatus* and *Candida tropicalis*. Gentamicin and Ketaconazole were used as positive controls to study the antibacterial and antifungal activities respectively. The antimicrobial activity of the test compounds was checked with various concentrations (25 µg/ml, 50 µg/ml and 100 µg/ml) against all the test pathogens. Each experiment was performed in triplicate and the results are represented as average zone of inhibition and minimum inhibitory concentration of all the test pathogens.

4.7. Cytotoxicity studies

Cytotoxic activity of the compounds was tested with human lung cancer cell lines A549, human breast cancer cell lines MCF-7 and human normal keratinocyte cells (HaCaT) by using MTT assay, which was done according to the earlier literature methods [70] and IC_{50} values obtained from nonlinear regression using GraphPad Prism 5 [71]. The LDH release [72] and NO release [73] assays of the compounds was evaluated by the earlier reported methods.

ACKNOWLEDGEMENT

The author G.K. greatly acknowledge **DST, New Delhi, India** for INSPIRE fellowship (IF140225 dated 23.01.2014). The author S.D greatly acknowledged **UGC, New Delhi, India** for UGC-BSR fellowship (F.25-1/2014-15(BSR)/7-26/2007(BSR) dated 05.11.2015).

Supporting information

Crystallographic data for the complex **1**, **2** and **4** have been deposited at the Cambridge Crystallographic centre as supplementary publication [1570688 (**1**), 1570689 (**2**) and 1570690 (**4**)]. The data can be obtained free of charge at w.w.w.ccdc.cam.ac.uk/conts/retrieving.html/

REFERENCES

1. M. Adams, Y. Li, H. Khot, C. De Kock, P.J. Smith, K. Land, K. Chibale, G.S. Smith, Dalton Trans. 42 (2013) 4677-4685.
2. P. Chellan, K.M. Land, A. Shokar, A. Au, S.H. An, C.M. Clavel, P.J. Dyson, C. De Kock, P.J. Smith, K. Chibale, G.S. Smith, Organometallics 31 (2012) 5791-5799.
3. B. Demoro, M. Rossi, F. Caruso, D. Liebowitz, C. Olea-Azar, U. Kemmerling, J.D. Maya, H. Guiset, V. Moreno, C. Pizzo, G. Mahler, L. Otero, D. Gambino, Biol. Trace Elem. Res. 153 (2013) 371-381.
4. A. Moreno-Rodríguez, P.M. Salazar-Schettino, J.L. Bautista, F. Hernández-Luis, H. Torrens, Y. Guevara- Gomez, S. Pina-Canseco, M.B. Torres, M. Cabrera-Bravo, C.M. Martinez, E. Perez-Campos, Eur. J. Med. Chem. 87 (2014) 23-29.
5. A. Walcourt, J. Kurantsin-Mills, J. Kwagyan, B.B. Adenuga, D.S. Kalinowski, D.B. Lovejoy, D.J.R. Lane, D.R. Richardson, J. Inorg. Biochem. 129 (2013) 43–51.
6. B. Ghosh, P. Adak, S. Naskar, B. Pakhira, P. Mitra, R. Dinda, S.K. Chattopadhyay, Inorg. Chim. Acta 459 (2017) 1-14.
7. R. Ramachandran, G. Prakash, S. Selvamurugan, P. Viswanathamurthi, J.G. Malecki, V. Ramkumar, Dalton Trans. 43 (2014) 7889-7902.
8. F.A. Beckford, J. Thessing, A. Stott, A.A. Holder, O.G. Poluektov, L. Li, N.P. Seeram, Inorg. Chem. Commun. 15 (2012) 225-229.
9. T.G. Kraljevic, A. Harej, M. Sedic, S.K. Pavelic, V. Stepanic, D. Drenjancevic, J. Talapko, S. Raic-Malic, Eur. J. Med. Chem. 124 (2016) 794-808.
10. P. Datta, A.P. Mukhopadhyay, P. Manna, E.R.T. Tiekink, P.C. Sil, C. Sinha, J. Inorg. Biochem. 105 (2011) 577-588.
11. B.S. Creaven, M. Devereux, D. Karcz, A. Kellett, M. McCann, A. Noble, M. Walsh, J. Inorg. Biochem. 103 (2009) 1196-1203.
12. A. Kulkarni, S.A. Patil, P.S. Badami, Eur. J. Med. Chem. 44 (2009) 2904-2912.
13. M.T. Klepka, A. Drzewiecka-Antonik, A. Wolska, P. Rejmak, K. Ostrowska, E. Hejchman, H. Kruszewska, A. Czajkowska, I. Młynarczuk-Biały, W. Ferenc, J. Inorg. Biochem. 145 (2015) 94-100.
14. H. Huang, P. Zhang, Y. Chen, K. Qiu, C. Jin, L. Ji, H. Chao, Dalton Trans. 45 (2016) 13135-13145.
15. P. Kalaivani, R. Prabhakaran, F. Dallemer, K. Natarajan, RSC Adv., 4 (2014) 51850-51864.

16. P. Kalaivani, R. Prabhakaran, E. Vaishnavi, T. Rueffer, H. Lang, P. Poornima, R. Renganathan, V. Vijaya Padma, K. Natarajan, Inorg. Chem. Front. 1 (2014) 311-324.
17. J.M. Rademaker-Lakhai, D. Van den Bongard, D. Pluim, J.H. Beijnen, J.H. Schellens, Clin. Cancer Res. 10 (2004) 3717-3727.
18. C.G. Hartinger, M.A. Jakupec, S. Zorbas-Seifried, M. Groessl, A. Egger, W. Berger, H. Zorbas, P.J. Dyson, B.K. Keppler, Chem. Biodivers. 5 (2008) 2140-2155.
19. G. Suess-Fink, Dalton Trans. 39 (2010) 1673-1688.
20. E. Jayanthi, S. Kalaiselvi, V. Vijaya Padma, N.S.P. Bhuvanesh, N. Dharmaraj, Dalton Trans. 45 (2016) 1693-1707.
21. B. Demoro, R.F.M. de Almeida, F. Marques, C.P. Matos, L. Otero, J.C. Pessoa, I. Santos, A. Rodriguez, V. Moreno, J. Lorenzo, D. Gambinoa, A.I. Tomaz, Dalton Trans. 42 (2013) 7131-7146.
22. B. Demoro, C. Sarniguet, R. Sanchez-Delgado, M. Rossi, D. Liebowitz, F. Caruso, C. Olea-Azar, V. Moreno, A. Medeiros, M.A. Comini, L. Otero, D. Gambino, Dalton Trans. 41 (2012) 1534-1543.
23. A. Garza-Ortiz, P. Uma Maheswari, M. Siegler, A.L. Spek, J. Reedijk, New J. Chem. 37 (2013) 3450-3460.
24. M.J. Chow, C. Licona, D.Y.Q. Wong, G. Pastorin, C. Gaiddon, W.H. Ang, J. Med. Chem. 57 (2014) 6043-6059.
25. S.W. Chang, A.R. Lewis, K.E. Prosser, J.R. Thompson, M. Gladkikh, M.B. Bally, J. J. Warren, C.J. Walsby, Inorg. Chem. 55 (2016) 4850-4863.
26. G. Kalaiarasi, S. Rex Jeya Rajkumar, S. Dharani, F.R. Fronczek, R. Prabhakaran, New J. Chem. 42 (2018) 336-354.
27. P. Kalaivani, R. Prabhakaran, P. Poornima, F. Dallemer, K. Vijayalakshmi, V. Vijaya Padma, K. Natarajan, Organometallics 31 (2012) 8323-8332.
28. A.B.P. Lever, Inorganic Electronic Spectroscopy, 2nd edn, Elsevier, New York, 1984.
29. A.A. Ali, H. Nimir, C. Aktas, V. Huch, U. Rauch, K.H. Schäfer, M. Veith, Organometallics 31 (2012) 2256-2262.
30. G. Kalaiarasi, Ruchi Jain, H. Puschman, S. Poorna Chandrika, K. Preethi, R. Prabhakaran, New J. Chem. 41 (2017) 2543-2560.
31. M. Adams, C. Kock, P.J. Smith, K.M. Land, N. Liu, M. Hopper, A. Hsiao, A.R. Burgoyne, T. Stringer, M. Meyer, L. Wiesner, K. Chibale, G.S. Smith, Dalton Trans. 44 (2015) 2456-2468.

32. J. Haribabu, K. Jeyalakshmi, Y. Arun, N.S.P. Bhuvanesh, P.T. Perumal, R. Karvembu, J. Biol. Inorg. Chem. 22 (2017) 461-480.
33. T. Sathiya Kamatchi, P. Kalaivani, P. Poornima, V. Vijaya Padma, F.R. Fronczek, K. Natarajan, RSC Adv. 4 (2014) 2004-2022.
34. G. Kalaiarasi, S. Rex Jeya Rajkumar, S. Dharani, J.G. Malecki, R. Prabhakaran, RSC Adv. 8 (2018) 1539-1561.
35. S. Mandal, D.K. Seth, P. Gupta, Inorg. Chim. Acta 397 (2013) 10-20.
36. A.M. Pyle, J.P. Rehmann, R. Meshoyrer, C.V. Kumar, N.J. Turro, J.K. Barton, J. Am. Chem. Soc. 11 (1989) 3051-3058.
37. A. Arshad, H. Osman, M.C. Bagley, C. Kit Lam, S. Mohamad, A.S. Mohd Zahariluddin, Eur. J. Med. Chem. 46 (2011) 3788-3794.
38. G. Devagi, G. Shanmugam, A. Mohankumar, P. Sundararaj, F. Dallemer, P. Kalaivani, R. Prabhakaran, J. Organomet. Chem. 838 (2017) 12-23.
39. G. Devagi, F. Reyhaneh, F. Dallemer, R. Jayakumar, P. Kalaivani, R. Prabhakaran, New J. Chem. 41 (2017) 8620-8636.
40. S. Satyanarayana, J.C. Dabrowiak, J.B. Chaires, Biochemistry 32 (1993) 2573-2584.
41. D. Suh, Y. Oh. J.B. Chaires, Process Biochem. 37 (2001) 521-525.
42. A. Chouai, S.E. Wicke, C. Turro, J. Bacsa, K.R. Dunbar, D. Wang, R.P. Thummel, Inorg. Chem. 44 (2005) 5996-6003.
43. J. R. Lakowicz, Principles of Fluorescence Spectroscopy, 2nd ed. Plenum Press, New York, (1999).
44. M.R. Eftink, C. A. Ghiron, Biochemistry, 15 (1976) 672-680.
45. J.R. Lakowicz, Principles of Fluorescence Spectroscopy, third ed., Springer, US, 2006.
46. P. Kalaivani, R. Prabhakaran, F. Dallemer, P. Poornima, E. Vaishnavi, E. Ramachandran, V. Vijaya Padma, R. Ranganathan, K. Natarajan, Metallomics 4 (2012) 101-113.
47. T.S. Morais, F.C. Santos, L. Corte-Real, M.H. Garcia, J. Inorg. Biochem. 129 (2013) 94-101.
48. T.E. Kydonaki, E. Tsoukas, F. Mendes, A.G. Hatzidimitriou, A. Paulo, L. Papadopoulou, D. Papagiannopoulou, G. Psomas, J. Inorg. Biochem. 160 (2016) 94-105.
49. F.F. Tian, F.L. Jiang, X.L. Han, C. Xiang, Y.S. Ge, J.H. Li, Y. Zhang, R. Li, X.L. Ding, Y. Liu, J. Phys. Chem. B 114 (2010) 14842-14853.

50. K. Tsai, T.G. Hsu, K.M. Hsu, H. Cheng, T.Y. Liu, C.F. Hsu, C.W. Kong, Free Radical. Biol. Med. 31 (2001) 1465-1472.
51. R. Prabhakaran, P. Kalaivani, R. Jayakumar, M. Zeller, A.D. Hunter, S.V. Renuka Devi, E. Ramachandran, K. Natarajan, Metallomics 3 (2011) 42-48.
52. P.G. Lawrence, P.L. Harold, O.G. Francis, Antibiot. Chemother. 4 (1957) 1980.
53. B.G. Tweedy, Phytopathology 55 (1964) 910-914.
54. R. Prabhakaran, A. Geetha, M. Thilagavathi, R. Karvembu, V. Krishnan, H. Bertagnolli, K. Natarajan, J. Inorg. Biochem. 98 (2004) 2131-2144.
55. K. Shanker, R. Rohini, V. Ravinder, P. Muralidhar Reddy, Y. Ho, Spectrochimica Acta Part A 73 (2009) 205-211.
56. J. Hildebrandt, H. Görls, N. Häfner, G. Ferraro, M. Dürst, I.B. Runnebaum, W. Weigand, A. Merlino, Dalton Trans. Comm. 45 (2016) 12283-12287.
57. S. Richter, S. Singh, D. Draca, A. Kate, A. Kumbhar, A.S. Kumbhar, D. Maksimovic-Ivanic, S. Mijatovic, P. Lönnecke, E. Hey-Hawkins, Dalton Trans. 45 (2016) 13114-13125.
58. L. Chen, F. Peng, G. Li, X. Jie, K. Cai, C. Cai, Y. Zhong, H. Zeng, W. Li, Z. Zhang, J. Chen, J. Inorg. Biochem. 156 (2016) 64-74.
59. K. Jeyalakshmi, J. Haribabu, N.S.P. Bhuvanesh, R. Karvembu, Dalton Trans. 45 (2016) 12518-12531.
60. C. Legrand, J.M. Bour, C. Jacob, J. Capiaumont, A. Martial, A. Marc, M. Wudtke, G. Kretzmer, C. Demangel, D. Duval, J. Hache, J. Biotechnol., 25 (1992) 231–243.b) E. Bonfoco, D. Krainc, M. Ankarcrona, P. Nicotera and S. A. Lipton, Proc. Natl. Acad. Sci. U. S. A., 16 (1995) 7162–7166.
61. L. Yu, P.E. Gengaro, M. Niederberger, T.J. Burke, R.W. Schriert, Proc. Natl. Acad. Sci. U.S.A. 91 (1994) 1691.
62. A.I. Vogel, Textbook of Practical Organic Chemistry, 5 th ed., Longman, London, 268 (1989).
63. S.K. Yusufzai, H. Osman, M. Shaheen Khan, S. Mohamad, O. Sulaiman, T. Parumasivam, J.A. Gansau, N. Johansah, H. Noviany, Med. Chem. Res. 26 (2017) 1139-1148.
64. N. Ahmad, J.J. Levision, S.D. Robinson, M.F. Uttley, E.R. Wonchoba, G.W. Parshall, Inorg. Synth. 15 (1974) 45-64.
65. G.M. Sheldrick, SHELXL-97, Program for Structure Refinement, University of Gottingen, Gottingen, Germany, 1997.

66. G.M. Sheldrick, SHELXL-2014/7: Program for the Solution of Crystal Structures, University of Gottingen, Gottingen, Germany, 2014.
67. M.S. Blios, Nature 29 (1958) 1199-1200.
68. P. Prieto, M. Pineda, M. Aguilar, Analytical Biochemistry 269 (1999) 337-341.
69. I. Weigand, K. Hilpert, R.E.W. Hancock, Nature Protocols 3 (2008) 163-175.
70. T.J. Mossman, Immunol. Methods 65 (1983) 55-63.
71. H.J. Motulsky, Prism 5 Statistics Guide, GraphPad Software Inc., San Diego, CA, 2007, http://www.graphpad.com.
72. W.E.C. Wacker, D.D. Ulmer, B.L. Vallee, J. Med. 255 (1956) 449-456.
73. D.J. Stueher, M.A. Marletta, J. Immunol. 139 (1987) 518-525.

HIGHLIGHTS

- Four new organoruthenium(II) complexes have been synthesized and characterized
- The DNA/protein interactions of ligands and complexes were studied by a variety of techniques
- The antimicrobial activity against four different bacteria and five fungi have also been examined
- The antiproliferative activity was evaluated against MCF-7 and HeLa cell lines
- The complexes **1-4** showed potent anticancer activity over the standard drug, *Cisplatin*
- Assay on HaCaT cell lines showed that the compounds were non-toxic to those cells.